Resolving Variations in the Tectonostratigraphic Terrane Structure of New England Using Receiver Functions

Author: John Joseph Schuh

Boston College Graduate School of Arts and Sciences
Department of Earth and Environmental Sciences

Resolving Variations in the Tectonostratigraphic Terrane Structure of New England using Receiver Functions

A Thesis by
JOHN SCHUH

Submitted in partial fulfillment of the requirements for the degree of
Master of Science

May 2014

Resolving Variations in the Tectonostratigraphic Terrane Structure of New England using Receiver Functions

by John Schuh **Advisor: John Ebel**

Abstract

Passive teleseismic data were collected with a 17-station broadband seismic array deployed from Vermont to Massachusetts. The purpose of the array was to detect changes in crustal seismic velocity structure related to the regional tectonostratigraphic terranes using receiver functions. Ps conversions from the Moho and mid-crust were observed and a cross-section of the crustal structure beneath the seismic array was produced. The crustal cross-section reveals a synclinal structure related to the Taconic orogeny, a remnant Iapetan oceanic slab, a plausible surface-location of the Red Indian Line, and several terrane boundaries that can be projected from their proposed surface locations into the deeper crust based on crustal-horizon offsets observed in the receiver function data.

Acknowledgments

I would like to thank Professor John Ebel for his advisement and oversight of this entire project. Thanks to the Weston Observatory for allowing me access to the seismic equipment that was necessary for data collection and thanks to the Weston Observatory staff for helping me manage the equipment. Thanks to Professor Charles J. Ammon for providing the receiver function programs essential to this research. Special thanks to Dr. Mike Hagerty who provided continuous IT support while getting the necessary Fortran computer programs properly installed on my computer. Thank you to my parents and fantastic friends for their love and support. Lastly, I would like to thank the following New England residents or businesses that allowed me to invade their home or office with seismic equipment:

David Ellis of Ellis Music

Herb L. Hohl III

Mascoma Valley Superintendent of Schools

The Selectmen of Grafton

John and Pat Lynch

Dale Randall

Bill and Michelle Brown

Colin and Julia Keenan

Charles and Patricia Twichell

Edgar and Coleen Thaxston

Royce and Susan Fuller

Table of Contents

List of Figures and Tables

1. INTRODUCTION

The Mohorovičić discontinuity, or Moho, marks the seismic boundary between the lower crust and upper mantle, where seismic P-wave velocity jumps from approximately 6.7 to 8.1 km/s. Because the Moho is included in the lithosphere, it can be deformed during collisional events between tectonic plates. This research focuses on the idea that the history of tectonic events (subduction, heating, uplift, etc.) that have transpired throughout time at a given location can be preserved in the deformation of the Moho. If this concept is true of the Northern Appalachians, then the depth and dip of both the Moho and mid-crustal features may be unique to individual tectonostratigraphic terranes and might be suggestive of certain types of crustal interactions between terranes (e.g., thrusting).

Much of the tectonic history of the New England tectonostratigraphic terranes is still in question (e.g., van Staal et al., 2009; Hatcher, 2010) and so far regional seismicity has not been linked with any active faults identified at the earth's surface (Ebel, 2007). Scientists have struggled to place locations of many New England terrane boundaries (e.g. Moench and Aleinikoff, 2003; Hepburn, 2006;) as well as struggled to understand the kinematics of terrane amalgamation (e.g., polarity of subduction, obduction of continental crust) that has occurred along the border of the North American Craton. By imaging the seismic structure of the earth's crust across the tectonostratigraphic terranes in New England, scientists may gain a better understanding of the constraints on the tectonic assembly of eastern North America, the location of terrane boundaries and/or crustal sutures in New England, and the relationship between crustal structure and regional seismicity.

To help address these questions that concern the New England terranes discussed in the previous paragraph, temporary seismic stations were deployed in a long transect that stretched

from central Vermont to eastern Massachusetts and an analysis of teleseismic data using a receiver function approach was applied to the seismic station data. Receiver function studies involve relatively low cost, passive-source (e.g., earthquakes) tomography methods that have been proven effective for imaging seismic discontinuities under a given seismic station (e.g., Li et al., 2002). The two most commonly used algorithms for creating receiver functions from teleseismic sources are **1)** the "water-level frequency domain deconvolution procedure" developed by Langston (1979) and **2)** the "iterative time-domain deconvolution procedure" developed by Ligorria and Ammon (1999). Both methods should produce nearly identical results to the other method, but factors such as wave propagation complications due to geology and noise contamination of the teleseismic signals may cause one method to outperform the other (Ligorria and Ammon, 1999).

This study makes use of results from both the water-level deconvolution and the iterative time-domain deconvolution procedures in an attempt to better constrain the receiver structure across the array. Receiver functions were created from data collected by temporary broadband seismic station deployments as well as by permanent New England Seismic Network (NESN) stations and the US National Seismic Network station HRV. Placement locations of the temporary stations that formed the seismic array were based on the preexisting locations of permanent network stations, boundaries between the New England tectonostratigraphic terranes, and the expected horizontal resolution achievable for a likely Moho depth in the region.

2. BACKGROUND

2.1 *Regional Geologic Setting*

The present day passive margin of New England and the Northern Appalachian Mountains is the result of at least three major orogenic events (Taconic, Acadian, and Alleghanian) that led to the accretion or formation of at least seven distinct terranes along the eastern margin of the North American Craton (Stroud, 2007; van Staal et al., 2009; Hatcher, 2010). These distinct landmasses, known as the New England tectonostratigraphic terranes (Figure 1), are distinguishable from each other by age and/or lithology and are typically bounded by fault zones (Zen et al., 1989; Hepburn et al. 1995, Stroud, 2007). While the orogenic events that accreted the terranes spanned much of the Paleozoic, the ages of some of the basement rocks of which the terranes are composed date back to the Precambrian (Zen et al., 1989).

2.2 *Summary of the Tectonostratigraphic Terranes*

The north-western-most terrane in New England that was accreted onto the North American craton is the Rowe-Hawley (aka the Witcomb Summit thrust or Baie Verte). The Rowe-Hawley (RH) is identified as an oceanic terrane derived from a back-arc basin that was obducted over the Laurentian margin (Grenville) during the Taconic Orogeny (van Staal et al., 2009). Immediately to the east of the RH is the Connecticut Valley Synclinorium (CVS), which is described as an extensional basin formed during rollback of an east-dipping subducting slab (Coish, 2010). The Bronson Hill (BH) terrane to the east of the CVS is identified as a volcanic arc that formed on either peri-Laurentian (ancient North American) or peri-Gondwanan (ancient African) crust above a west-dipping subduction zone (Karabinos et al., 1998; van Staal et al., 2009). The locations of these terranes in New England are shown in Figure 1.

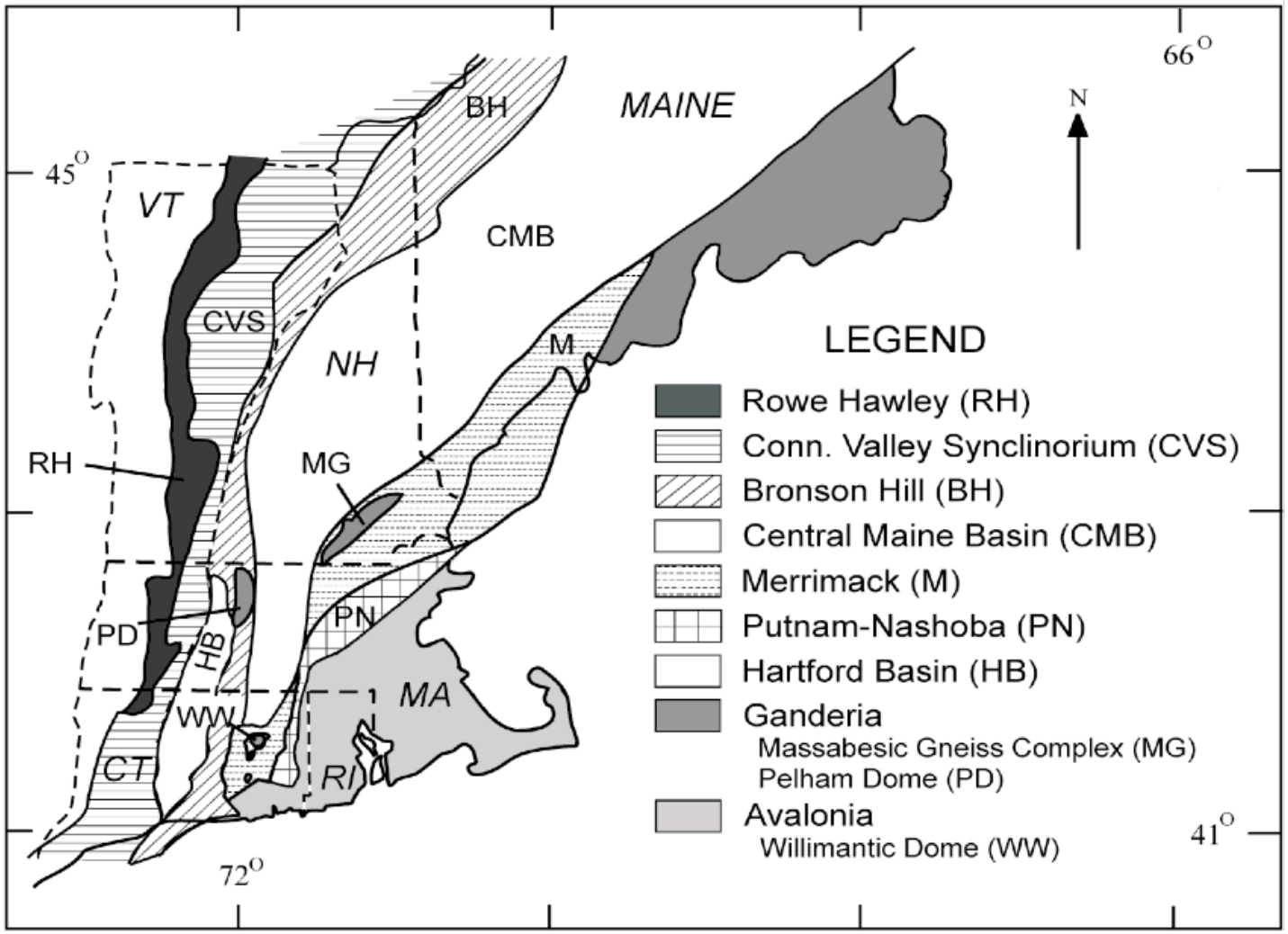

Figure 1. Map of the New England Tectonostratigraphic Terranes. From Dorias et al., (2009).

The Central Maine Basin (CMB) terrane, which is part of a larger Laurentian-amalgamated peri-Gondwanan microcontinent known as Ganderia, makes up the western margin of Ganderia where an oceanic slab is believed to have subducted under Laurentia prior to continent docking (van Staal, 2009). Along the eastern margin of Ganderia is the Merrimack terrane, which is separated from the Central Maine terrane to the west by a complex zone of faults (Zen et al., 1989) as well as by a difference in continental sediment derivation of surficial rocks (Hussey et al., 2010; Dorais et al., 2009). The basement rocks for both of these terranes is thought to be of latest Proterozoic age (van Staal et al., 2009).

The Merrimack terrane and Putnam-Nashoba (PN) terrane are separated by the Clinton-Newbury fault, which was demonstrated, using gravity data, to be dipping to the west (Fisk, 1985). The PN terrane is classified as an early Paleozoic arc that was located on the overriding plate of a subduction zone with either the Merrimack slab or Avalon slab or both acting as the subducting plate(s) (Hepburn, 2006; Stroud, 2007). The Bloody-Bluff fault separates the PN terrane to the northwest from the Precambrian volcanic and sedimentary rocks of the Avalon terrane to the southeast (Stroud, 2007). The Bloody-Bluff fault has been interpreted as having both thrust and strike-slip components of motion, which is suggestive of an oblique continental convergence between the two terranes (Bell, 1968; Skehan, 1969). The van Staal et al. (2009) model for the Acadian Orogeny describes subduction of the Avalonian oceanic slab under Ganderia, which resulted in partial obduction of Ganderia over Avalon.

2.3 *Statement of the Research Problem*

There are still unresolved questions concerning the assembly of the various tectonostratigraphic terranes of the Northern Appalachian Mountains. These questions concern determinations of the timing of accretion, the direction (polarity) of subduction, continental

affinity (i.e., peri-Laurentian vs. peri-Gondwanan), and the location of major crustal sutures (e.g., Moench and Aleinikoff, 2003; Hepburn, 2006; van Staal et al., 2009; Hatcher, 2010). Further insight into the crustal assemblage of the terranes, the location of major crustal sutures (e.g., the principle Iapetan suture), and subduction processes (e.g., polarity) between the terranes may be achieved using seismic imaging methods to determine the structural characteristics of both the Moho and major crustal features (faulting) across the tectonostratigraphic terranes.

In addition to the uncertainties associated with the assembly of the terranes, the relationship between modern seismicity and regional geological features (Figure 2) is currently poorly resolved in New England, i.e., no active faults have been identified, but earthquakes do occur (Ebel, 2007). Studying the structural variations in the deep crust of the New England terranes might reveal seismically active features that are only visible at depth.

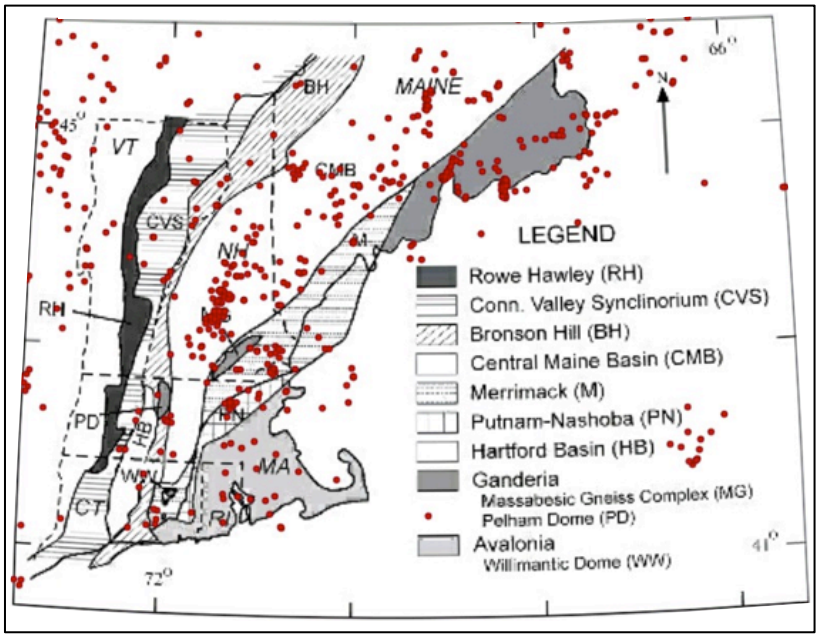

Figure 2. Earthquake epicenters in New England from 1990-2011 as reported by the Weston Observatory. Epicenters are shown as red dots. Terrane boundaries correspond with major fault zones as mapped at the earth's surface.

2.4 *Previous Studies on the Seismic Structure of New England*

Moho offset and large fluctuations in crustal thickness (e.g., ≈20km vertical change over ≈100km laterally) are typically observed in active plate boundary settings (Yamauchi et al., 2003; Di Stefano et al., 2011), but isostatically coupled surface erosion and lower crust-upper mantle ductile flow tend to mitigate these features over geologic time in tectonically less active settings (Kusznir and Matthews, 1988). Since the most recent known active tectonic event in New England occurred during the Mesozoic (≈100 Ma), and the most recent orogenic event in New England ended in the late Paleozoic (≈260 Ma), it is conceivable that crustal thickening and/or Moho offsets related to these past tectonic events are no longer detectable in the modern Moho and crustal thickness of the region. On the other hand, some seismic studies that have imaged the lower crust and upper mantle in ancient orogenic zones have suggested that crustal thickening and Moho offset related to ancient events, in some cases as old as Precambrian, can be preserved to the present (Doll et al., 1996; Korsch et al., 1997; Diaconescu et al., 1998). Therefore, while Moho offset and crustal thickness related to tectonic interactions between the New England terranes have no doubt diminished over time, it is possible that crustal thickness and offsets related to the ancient tectonic events in New England are detectable using seismic imaging methods.

The Doll et al. (1996) east-central Maine reflection study is of interest to this study because a sharp, vertical Moho offset associated with the Norumbega Fault Zone (NFZ) is observed. While not considered to be a terrane boundary, the NFZ is one of the largest fault systems in the northern Appalachians, and is considered to be a Paleozoic analog to the modern San Andreas Fault (Doll et al., 1996). The combination of geologic mapping and seismic data from the NFZ suggest that this middle-to-late Paleozoic fault zone experienced slip reactivation

during regional Mesozoic (or younger) extension (Doll et al., 1996). This finding suggests that other relatively old major crustal sutures in New England (e.g., terrane boundaries) might have gained some offset with the assistance of younger regional tectonic events (e.g., Mesozoic extension), increasing the likelihood that detectable Moho offsets between terrane boundaries still exist, and therefore might be imaged by the teleseismic receiver structure methods.

Several deep crustal seismic reflection and refraction studies have been completed in the Northern Appalachian Mountains (e.g., Ando et al., 1984; Hughes and Luetgert, 1991; Doll et al., 1996; Zhu, 1996). Ando et al. (1996) and Hughes and Luetgert (1991) both model a prominent east-dipping midcrustal penetrating ramp in western New England, which is interpreted as the boundary between the accreted Appalachian terranes and the Grenvillian lithologies of the North American craton, but neither study observed variations in structure of the New England crust that could be directly correlated with tectonostratigraphic terrane boundaries. However, alternative seismic imaging methods are available that might be better suited for imaging the deep crust (e.g. receiver functions), where evidence of certain types of tectonostratigraphic terrane interactions (e.g. thrusting) may exist. The Ando et al. (1984) and Hughes and Luetgert (1991) seismic lines did not reach into the eastern Merrimack, Nashoba, and Avalon terranes of New England (Figure 3) and while Zhu (1996) identified variations in Moho depth associated with surficial geologic features in Northern New England (e.g., the Chain Lakes Massif and White Mountain Batholith), reflection midpoints are relatively sparse and no data exist south of the northern Massachusetts state border. Further research is therefore needed to investigate what types of deep crustal structures exist in the southeastern portion of New England.

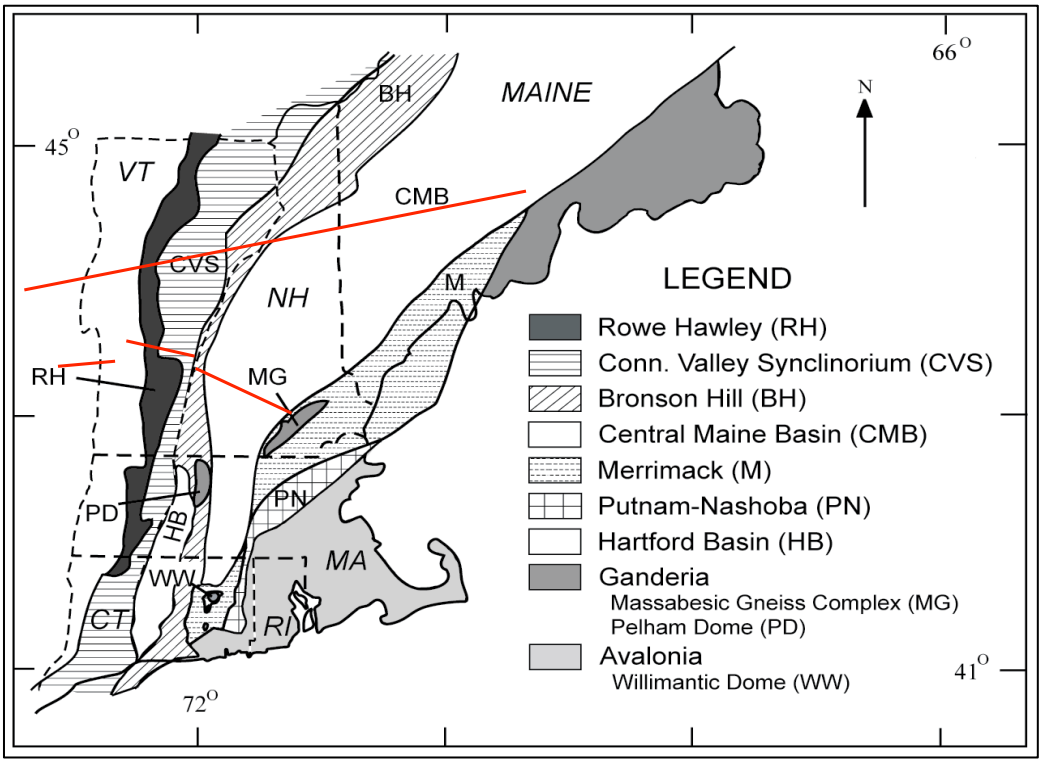

Figure 3. Red lines indicate the locations of Hughes and Luetgert (1991) and Ando et al. (1984) seismic reflection lines. Neither study reached into the Merrimack, Putnam-Nashoba, or Avalon terranes.

In addition to the relatively high-resolution seismic reflection and refraction surveys performed in New England, there have also been numerous crust and upper-mantle velocity models developed in New England using seismic tomography methods that employ regional and teleseismic body waves (e.g., Taylor and Toksöz, 1979; Foley, 1984; Zhu and Ebel, 1994; Li et al., 2002). The scale of the numerous velocity models developed in these studies ranges from the whole of New England to specific locations beneath particular seismic stations. Comparison of the different velocity models from these other studies suggests that crustal thickness in New England ranges from ≈29km to ≈40 km, the thinnest of which is beneath the Avalon terrane (Foley, 1984).

All of the abovementioned seismic experiments in the Northern Appalachians have provided useful information on the crustal structure in New England, but studies with higher spatial resolution are required to decipher localized transitions from one geologic terrane to another, particularly for the easternmost terranes of southern New England, in which very few seismic studies have been performed. Additional information collected on the structure of the deep crust in New England could resolve quandaries such as those over the subduction processes associated with the Nashoba terrane, the location of the principal Iapetan suture in New England and potential deep crustal features that may spatially correlate with seismicity in New England. This information can be collected using seismic tomography methods to image the shape (e.g., synclinal or anticlinal) and dip of crustal features (i.e., the Moho and mid-crustal layers/ horizons) of the tectonostratigraphic terranes, which is crucial to understanding the region's tectonic history and current crustal assemblage.

3. METHOD

3.1 *Receiver Functions*

Receiver function (RF) methods have proven effective in determining depth and topography of seismic interfaces within the earth (e.g., Langston, 1979; Ligorria and Ammon, 1999), especially those discontinuities that separate layers of very different acoustic impedance such as the Moho, which separates the relatively low density crust (2.7 g/cm^3) from the much higher density Mantle (3.3 g/cm^3). Receiver functions (RFs) can also be sensitive to (i.e., detect) at least one midcrustal reflector and have been used to create crustal cross-sections in various regions (e.g., Gilbert, 2012). The data needed to create RFs are the initial P wave and P-

wave coda from teleseismic events. Typically, teleseismic events used in receiver-function studies are restricted to those events that occur between 30° and 95° away from the seismic station. This distance range for teleseisms is that range in which the direct P wave from a seismic source samples the structure beneath the seismic station while avoiding near-source effects and interaction with the outer-core (Langston, 1979). A RF is based on the idea that the waveform of a three-component seismogram of a teleseismic earthquake is the result of three effects: the source signal from the earthquake (source-time function), the signal from the earth structure below the seismic station, and the instrument response (impulse response) of the seismometer (Stein and Wysession, 2003). This relationship can be expressed as a convolution of the three signals in the time domain as

$$D(t) = S(t) * E(t) * I(t) \qquad (1)$$

where $S(t)$ is the source signal, $E(t)$ is the response to the earth structure along the path of the seismic waves, $I(t)$ is the impulse response of seismometer, and $D(t)$ is the seismogram. A RF is the result of the deconvolution of the source and instrument signals from the seismogram so that only the near-receiver earth structure response remains. If Equation 1 is expressed in the frequency domain, then the frequency response of the earth can be given as

$$E(\omega) = \frac{D(\omega)}{I(\omega)S(\omega)} \qquad (2)$$

for either the vertical or radial component of the seismogram. The source equalization receiver function method developed by Langston (1979) employs the frequency domain water-leveled deconvolution technique described by Clayton and Wiggins (1976). In this procedure, the

Fourier transform of the radial receiver function, $H(\omega)$, is given as

$$H(\omega) = \frac{R(\omega)Z^*(\omega)}{\phi(\omega)} G(\omega) \qquad (3)$$

where $R(\omega)$ is the Fourier transform of the radial component of motion, $Z^*(\omega)$ is the complex conjugate of the Fourier transform of the vertical component, $\phi(\omega)$ is the autocorrelation of the vertical component with spectral troughs filled to a water-level parameter, and $G(\omega)$ is a Gaussian filter with a predetermined width parameter (Ammon, 1991). In general, a higher value of the Gaussian filter width parameter will produce a higher vertical resolution image of the subsurface (the receiver function). However, a higher frequency RF can also include more high frequency noise, which reduces the signal-to-noise ratio (SNR) and thus the quality of the RF.

A good estimation of the RF can be achieved through the iterative time-domain deconvolution process developed by Ligorria and Ammon (1999). The RF in this case is the result of a least-squares minimization of the difference between the observed horizontal seismogram and a predicted signal generated by the convolution of an iteratively updated spike train with the vertical component seismogram (Ligorria and Ammon, 1999). The iterative time domain method predicts the radial RF using a series of Gaussian pulses whose width parameter must be set a priori. The series of pulses is then convolved with the recorded vertical seismogram to produce a radial seismogram. Successive pulses are iteratively added until the misfit between the observed radial seismogram and the predicted seismogram reaches a user-defined misfit percentage or until a pre-defined maximum number of iterations have been executed (Eager et al., 2010). The theory behind any RF approach to analyzing earth structure is illustrated in Figure

4. The phase arrivals after the direct P wave are all S waves converted from direct P (Ps) or P-to-S multiples.

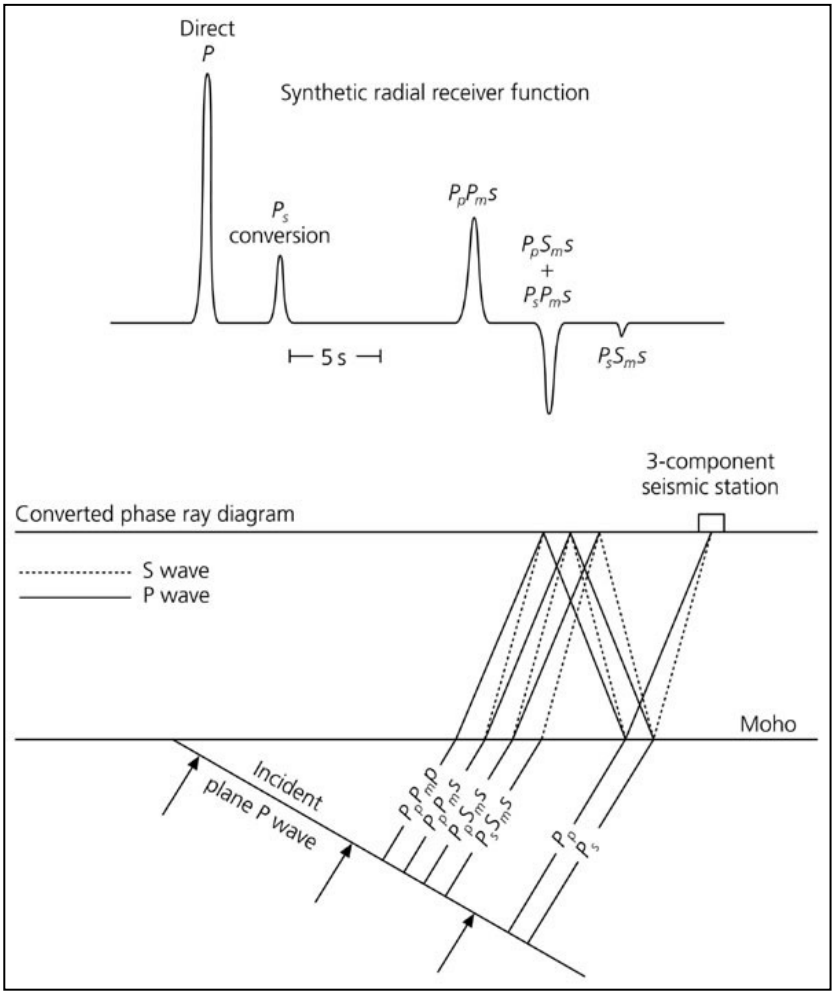

Figure 4. Diagram of the receiver function approach. The resulting seismogram should have arrivals of seismic wave phase changes as they encounter an interface below the receiver. The Moho is used as the seismic interface in this example but the theory remains the same for any acoustic impedance interface encountered by a teleseismic P wave. From Stein and Wysession (2003).

While classical receiver function studies have generally focused on complicated and time-consuming forward modeling and receiver function inversion to obtain a velocity structure

(e.g., Langston, 1979), many contemporary RF array studies have focused on creating 2-D cross sections of the crust and lithosphere by interpreting only the direct Ps conversions (e.g., Yamauchi et al., 2003; Di Stefano et al., 2011; Gilbert, 2012). Cross sections are created for RF arrays by performing moveout corrections on individual RFs. The moveout corrections are based on event ray-parameter (See Appendix 1). For events of differing ray-parameter, the moveout correction should align direct Ps conversions while reverberations should fall out of phase (Mohsen, 2004). The maximum difference in arrival time due to ray parameter moveout is about 0.25 seconds for a Ps conversion from the Moho assuming ak135 velocity model parameters (Kennett, 2005). The resulting RF profile is similar to a seismic reflection profile; the only difference is that the arrivals after time-zero on the RF profile are converted P-to-S-wave transmissions (Ps) from layer boundaries instead of P-wave reflections (Figure 5).

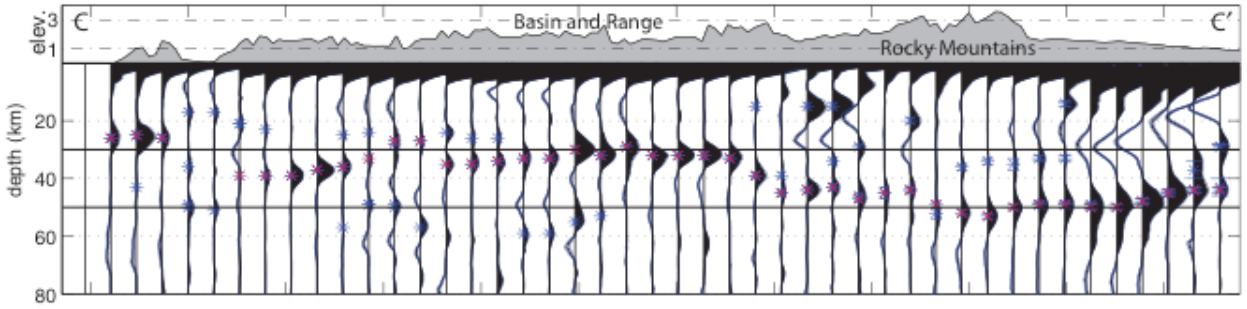

Figure 5. Example of how receiver function arrays are used to create structural cross-sections of the crust using the Ps conversions. Time in a receiver function is converted to depth using a velocity model and then the direct P wave is placed at the surface of the earth while the wave conversions (Ps) that follow the direct P wave represent layers within the earth. From Gilbert (2012).

3.2 *Data Collection*

A passive-source seismic array was designed to image the crustal structure across the tectonostratigraphic terranes of southeastern New England (Figure 6). The array consisted of thirteen (13) temporary seismic stations, three (3) New England Seismic Network (NESN) stations, and the US National Seismic Network station HRV. The selection of temporary seismic station locations was based on the location of the tectonostratigraphic terranes and their boundaries, the locations of the permanent seismic network stations, and the horizontal resolution achievable by RF methods applied to the lower crust. The available number of portable seismic station equipment was limited, and the temporary station deployment periods were not uniform across the array (i.e., data collection periods/ dates were not the same for each temporary station).

Compared to active-source seismic studies, whose data can be collected relatively quickly (hours to days), passive-source seismic studies typically require longer deployment periods (a few months to years). The available temporary seismic stations for this study were deployed for ≈3-5 months and then moved to different predetermined locations (See Appendix 2). The temporary seismic stations consisted of a 3-component Guralp CMG-40T portable broadband seismometer, a RefTek RT-130 data acquisition system, and a GPS transceiver. The seismometers were oriented to true north, sampled at 40Hz, and the data were saved in RefTek format.

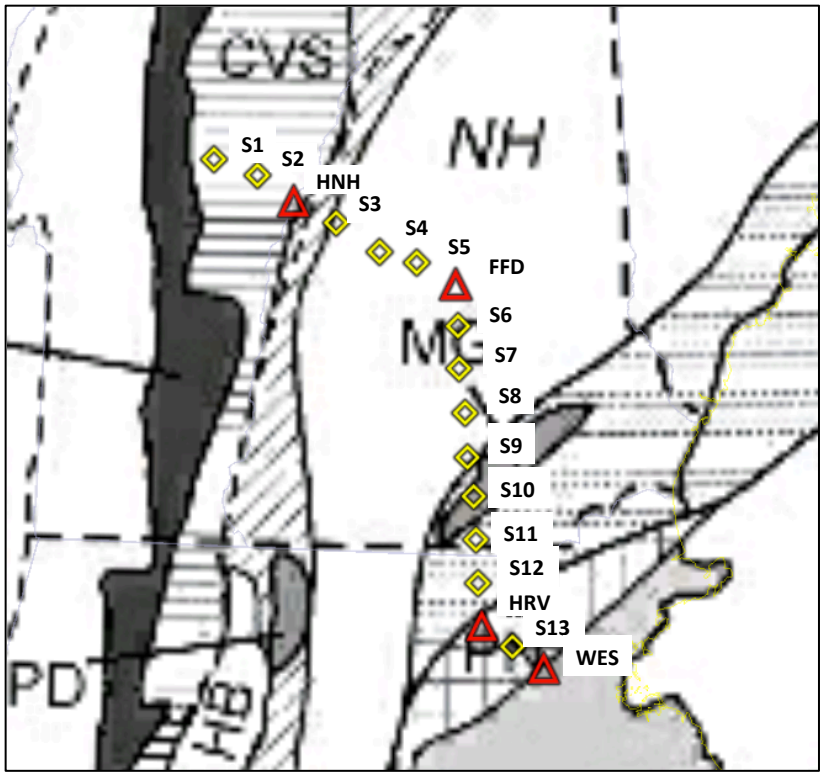

Figure 6. Map showing the seismic array that was deployed for this study. The array was designed to detect changes in velocity structure from one terrane to the next using receiver functions. Yellow diamonds indicate temporary seismic stations. Red triangles indicate permanent seismic network stations. Each station is labeled with its station name.

3.3 *Data Processing*

Using the Seismic Analysis Code (SAC, © 1995 Regents of the University of California), seismograms were assembled from the data collected at each station in the seismic array. Only events of magnitude 5.7 or greater that were at epicentral distances between 30° and 95° away from the receivers were considered for the RF analysis. For each individual event the seismograms were windowed ±60 seconds around the theoretical P wave arrival time. The windowed seismograms were linear-trend corrected and mean-removed. The seismograms were

then bandpass filtered from 0.4-1.5Hz, which is within the expected body wave frequency for teleseisms (Foley, 1990; Levander, 2003). The 3-component seismograms were tapered at the extremities and then the horizontal components were rotated to the radial and tangential components of motion for each specific event. Receiver functions were then produced using the Receiver Function Analysis Computer Programs provided by Professor Charles J. Ammon (Penn State).

Both the water-level frequency domain deconvolution (Langston, 1979) and iterative time domain deconvolution (Ligorria and Ammon, 1999) methods were employed. The two methods should produce nearly identical results to each other, but factors such as wave propagation complications due to geology and data quality reduction due to noise contamination of the teleseismic signals may cause one method to outperform the other (Ligorria and Ammon, 1999).

RFs generated for this study using the Langston (1979) method had a water-level of 0.01 for the spectral troughs and a Gaussian width parameter of 2.5, both of which are commonly used values in crustal receiver function studies (e.g., Langston, 1979; Ligorria and Ammon, 1999; Li et al., 2002; Yamauchi et al., 2003). RFs generated for this study using the Ligorria and Ammon (1999) method applied a Gaussian width parameter of 2.5, and the program was allowed to iterate until a misfit of 0.001% was obtained or 200 iterations were reached. The Gaussian width parameter of 2.5 used in each method translates to an approximate pulse width of 1 second (Ammon, 1997).

RFs at each station were grouped by back azimuth (BAZ) and placed into ±0.05 s/km ray parameter bins for stacking (See Appendix 3). Final receiver function stacks were moveout corrected to a ray parameter of 0.06 s/km based on the expected Ps Moho conversion using

average ak135 velocity model parameters for the crust and upper mantle (Appendix 1). Ps arrival times for the Moho and crust were depth transformed and the theoretical Ps conversion point coordinates were calculated. Ps conversion points were organized into three transects, plotted in cross section, and interpreted.

4. RESULTS AND INTERPREATION

The final RF dataset (Figure 7) consisted of two RFs at each station from different back azimuths (BAZs), with the exception of Station 4 (only 1 RF) and Station 13 (3 RFs). The method for selecting RFs for final analysis is discussed in Appendix 3. Figure 7 shows the results from both the water-level deconvolution and iterative time domain deconvolution RF methods. Each RF is moveout corrected to a ray parameter of 0.06 s/km and is windowed from -2 sec to +8 sec around the P-wave arrival. Assuming ak135 crustal thickness and velocities, the direct Ps Moho conversion (PmS) should lag the direct P wave by ≈4 seconds. The Moho is clearly imaged across most of the array in this study, with PmS conversions arriving between 3-5 seconds after the direct P wave. Crustal Ps conversions (PcS) are seen between 1-3 seconds after the P-wave arrival and appear to be more prominent and traceable across the array when the water-level deconvolution (Langston, 1979) is applied. Arrivals that come after the PmS in Figure 7 are considered to be crustal multiples.

PmS and PcS arrival times were picked from each RF method in Figure 7. The arrival picks for the water-level method were averaged with the arrival picks from the iterative time domain method, converted to depth using the ak135 velocity model, and the theoretical conversion point latitudes and longitudes were calculated. Figure 8 shows the theoretical Moho Ps conversion points in map view as determined from the BAZ of each event used in the final dataset. The conversion points were organized into three separate linear transects (indicated by

color and shape on Figure 8) that were utilized for cross-section analysis. The location (latitude, longitude, depth) of the points were plotted in cross section with vertical and horizontal error bars determined by the Rayleigh criterion (vertical resolution) and Fresnel Zone (horizontal resolution), respectively (Figure 9; Appendix 4).

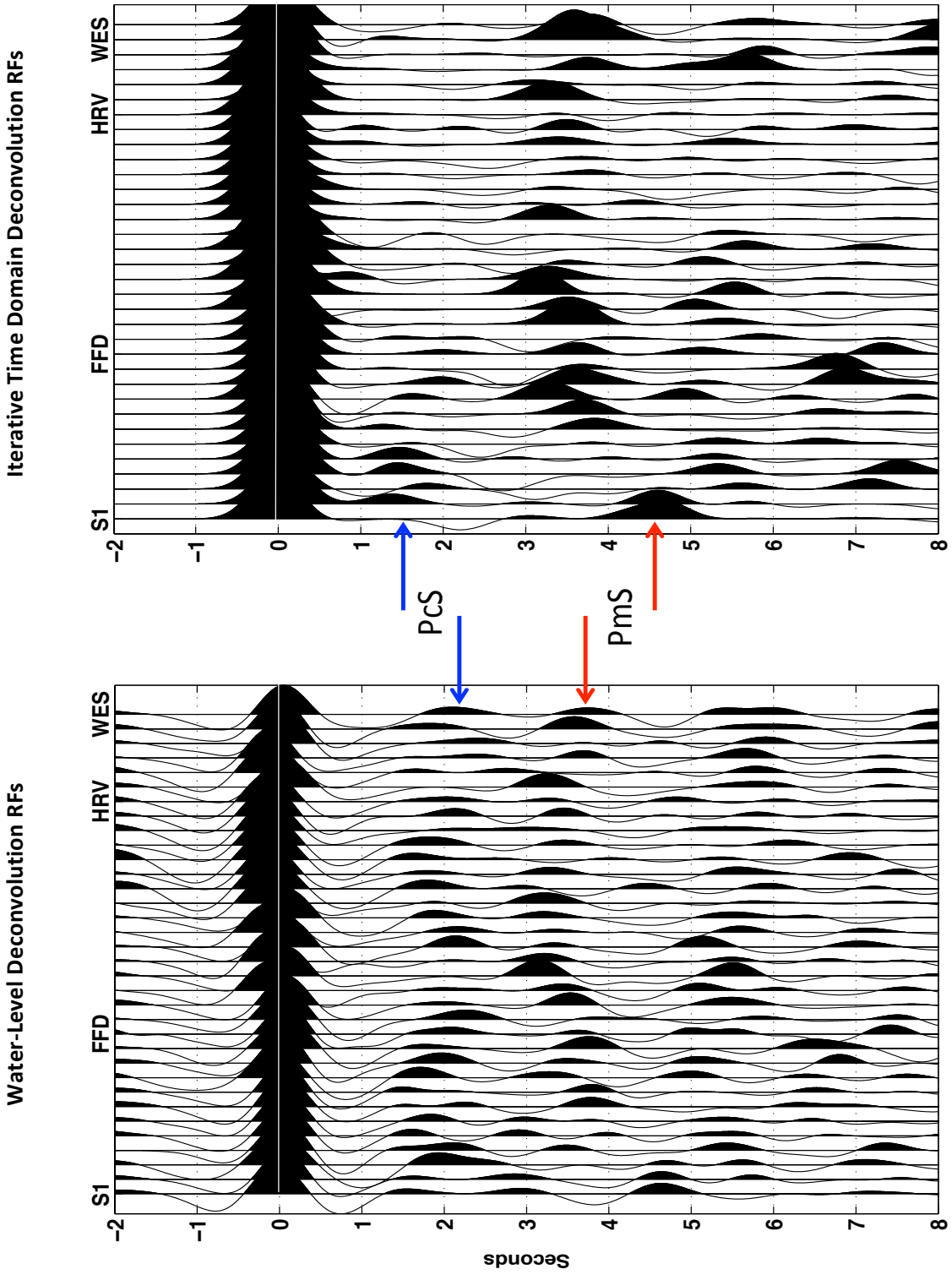

Figure 7. Comparison of final water-level deconvolution (left) and iterative time-domain deconvolution (right) receiver functions. RFs are displayed from approximately northwest to southeast. Stations corresponding with corners in the array are shown at the top of each figure. PmS conversions arrive between 3-5 seconds (red arrows). PcS conversions arrive between 1-3 seconds (blue arrows) and are less apparent when the iterative time-domain deconvolution is applied.

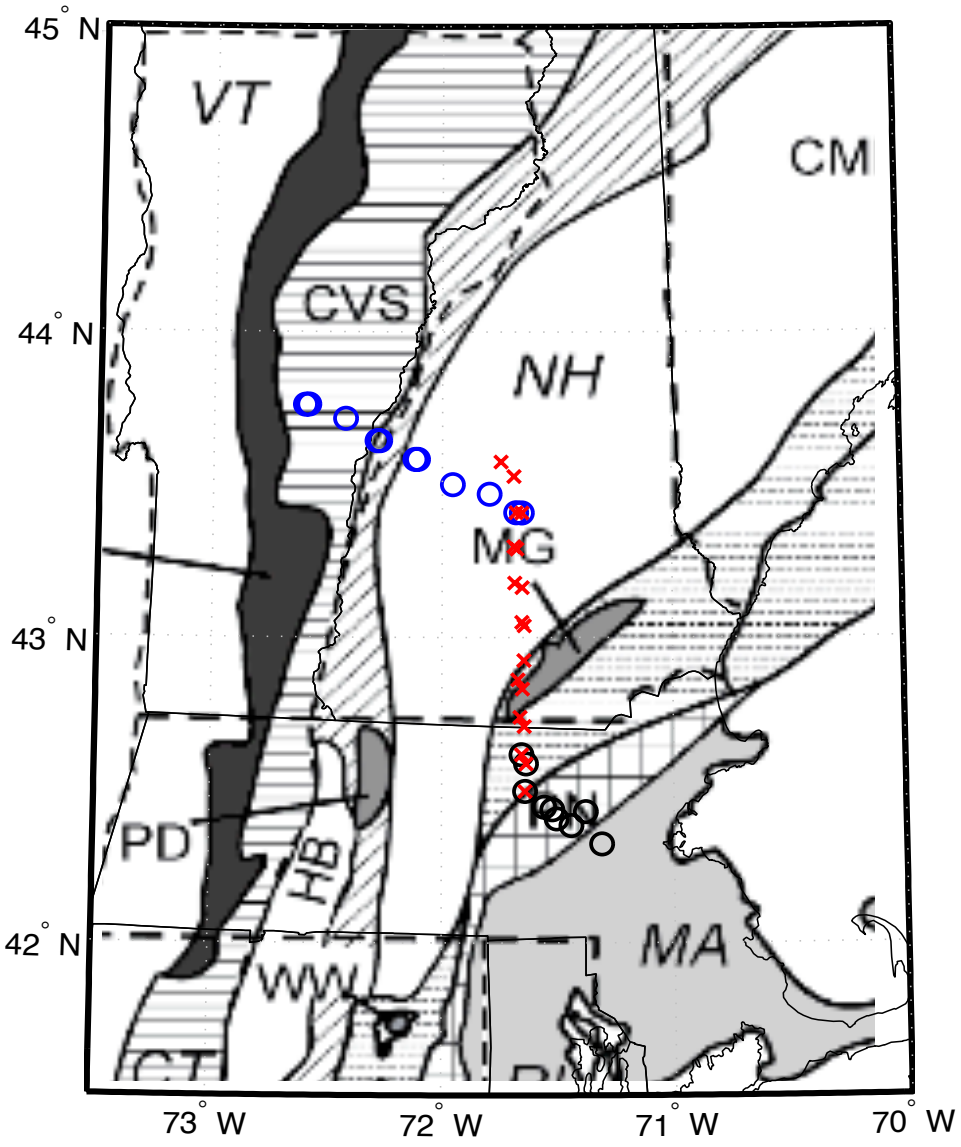

Figure 8. Map showing the theoretical Moho Ps conversion points based on event BAZ and a ray parameter of 0.06 sec/km. Point size is arbitrary and not related to horizontal resolution. Conversion points are organized into Transects 1, 2, and 3: Transect 1 in the north is shown as hollow blue circles; Transect 2 in the center is shown as red X's; Transect 3 in the south is shown as black hollow circles. Some points are used in more than one transect.

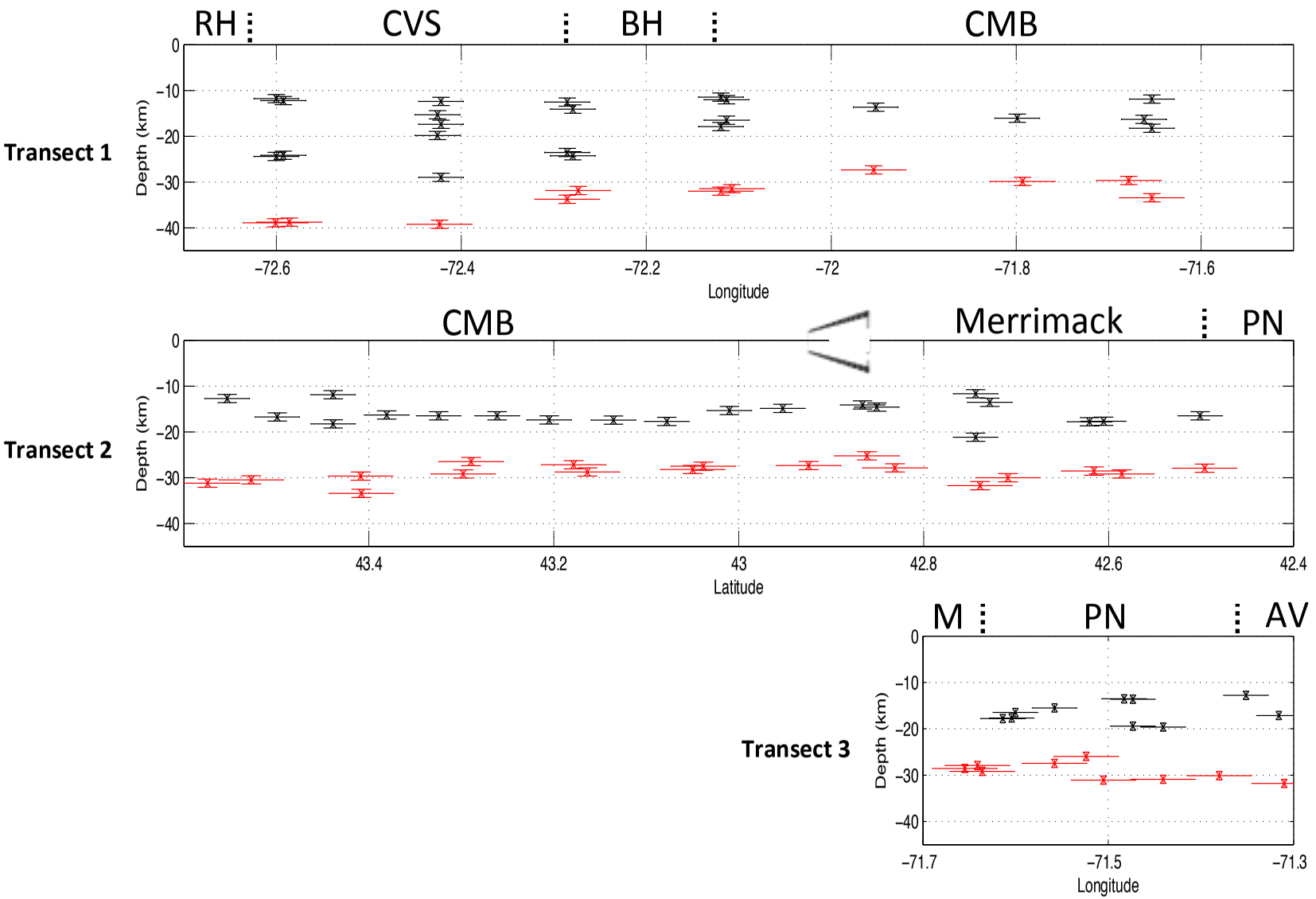

Figure 9. PmS and PcS conversion point depths for all three transects in the seismic array. PcS points are colored black while PmS points are red. Points are plotted with vertical and horizontal error bars as determined by the horizontal and vertical resolution. Transect 1 and Transect 3 conversion points are plotted vs. longitude and Transect 2 conversion points are plotted vs. latitude. Surface locations of terrane boundaries are shown on the top of each transect. The CMB-Merrimack boundary in Transect 2 is shown at angle.

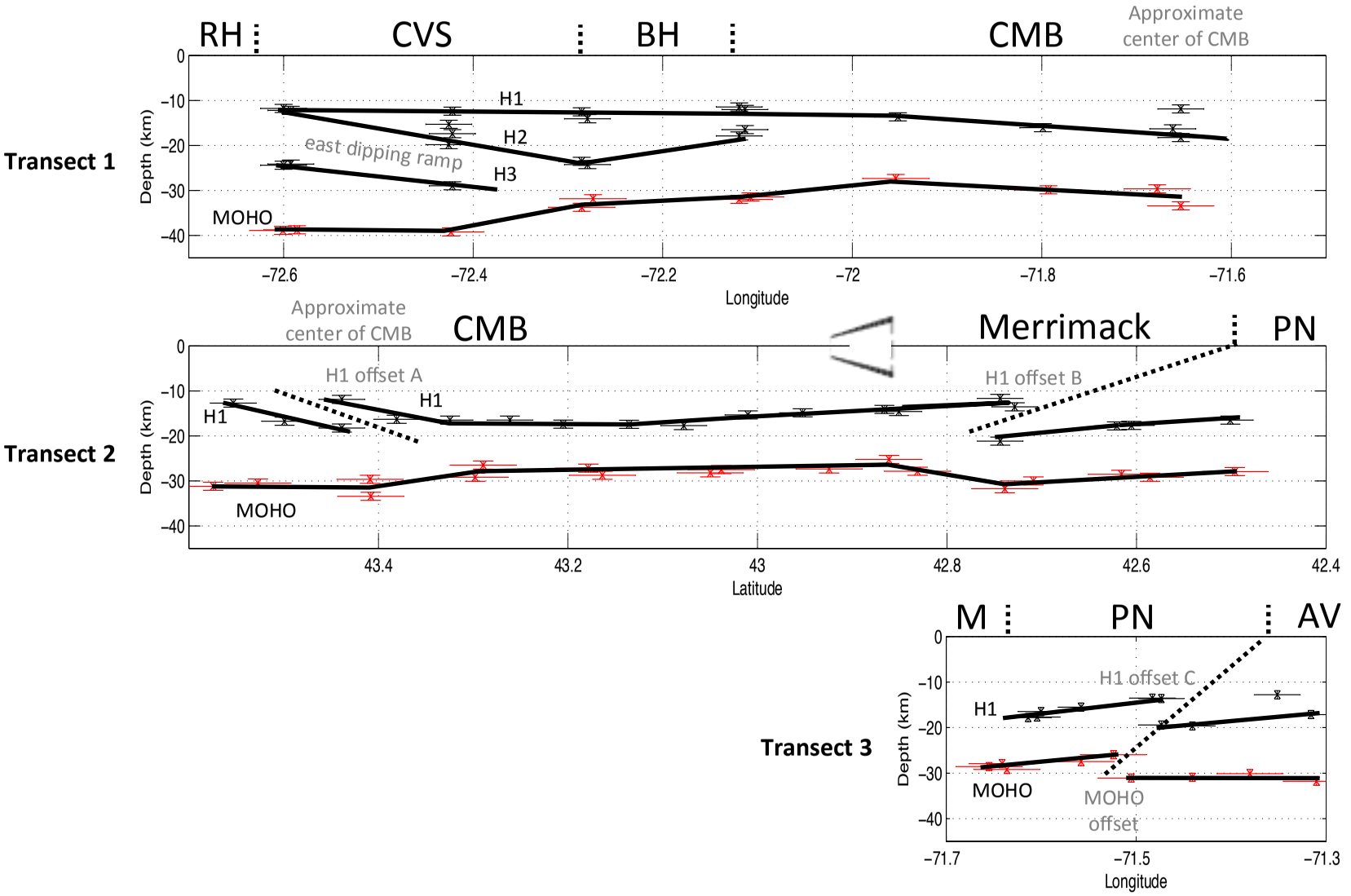

Figure 10. Interpretation of Figure 9. See text for discussion.

The Ps conversions from Figure 9 are interpreted in Figure 10. Crustal thickness in the region is found to be deepest beneath the northwestern portion of the array (western section of Transect 1) and shows a general thinning toward the east, which is consistent with the findings of Hughes and Luetgert (1991) and Zhu (1996). Crustal thickness appears to change most rapidly (from ≈40 to ≈30 km) between the RH-CVS boundary and the BH-CMB boundary as seen in Transect 1, which is expected as the crust transitions from thicker North American Craton (Laurentia) to the thinner accreted Appalachian terranes (Li et al., 2002).

In Transect 1 on Figure 10, three separate crustal horizons (H1, H2, and H3) are interpreted beneath the surface boundaries of the CVS, two of which (H2 and H3) dip apparently to the east on the western end of the transect. An east dipping mid-crustal ramp that extends beneath the CVS has been observed in previous reflection studies (e.g., Hughes and Luetgert, 1991; Ando et al., 1984) and was interpreted by those researchers to be the western boundary of the accreted Appalachian terranes, which were thrust over Grenville during the Taconic Orogeny. The shallowest crustal horizon observed in Transect 1 (H1) appears to be continuous across the CVS-BH and BH-CMB terrane boundaries. Both H1 and the Moho take on an apparent easterly dip in the CMB in Transect 1. The H2 crustal horizon in Transect 1 is interpreted here to have a synclinal "V" shape. The synclinal "V" shape of the H2 crustal horizon is seen within the mid-crust of the CVS and Bronson Hill terranes, and suggests up-thrusting of the margins of these terranes over the regions of crust immediately to the east and west, resembling a type of crustal wedge. Crustal wedging of the CVS and Bronson Hill is consistent with the tectonic model for the evolution of the Shelburne Falls Arc (located on western edge of the CVS, east of the RH) and Bronson Hill Arc (currently to the east of the CVS) discussed by Karabinos et al. (1998) and Dorias et al. (2008). The tectonic model described by the authors

mentioned in the previous sentence includes east-dipping subduction of the Neo-Iapetus Ocean under a continental fragment located to the east of the Neo-Iapetus during the early Ordovician period, followed by the west-dipping subduction of the Iapetus Ocean under the same continental fragment during the late Ordovician period (Figure 11). As the continental fragment was wedged between Laurentia and the Iapetus Ocean, the east-dipping subduction beneath the west side of the continental fragment and west-dipping subduction beneath the east side of the continental fragment would have resulted in up-thrusting of both margins of the crustal fragment. These tectonic processes could have resulted in synclinal or "V" shaped horizons within the CVS and Bronson Hill terrane crust, much like the "V" shaped H2 horizon in Figure 10.

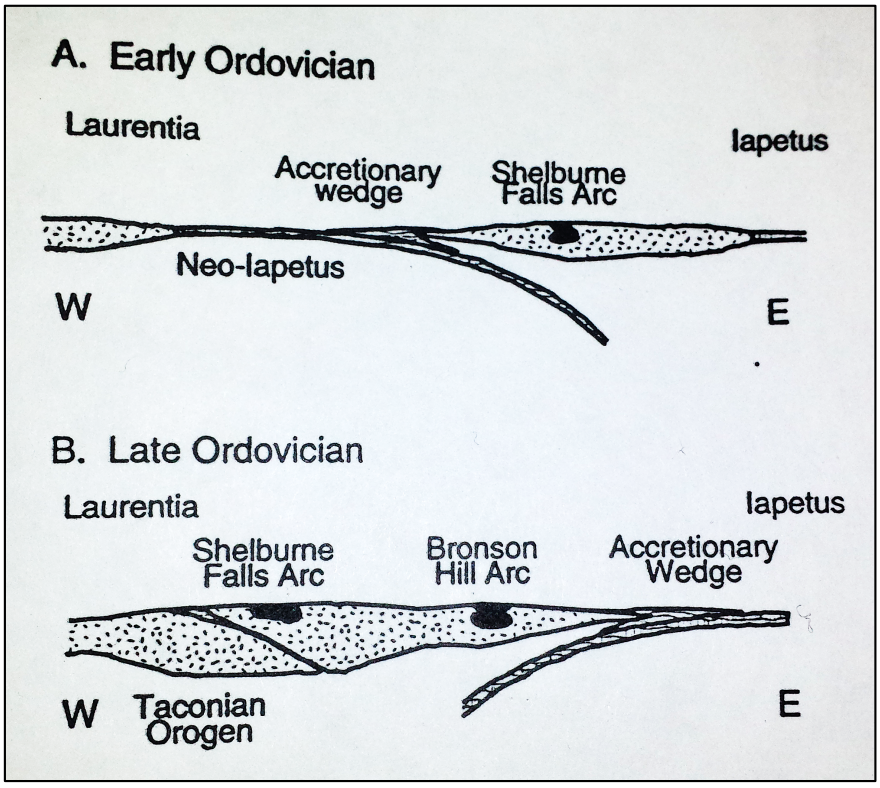

Figure 11. Cross-section model for the tectonic evolution of a continental fragment upon which the Shelburne Falls Arc and Bronson Hill Arc are proposed to have formed. Subduction of the Neo-Iapetus Ocean under the continental fragment followed by subduction of the Iapetus Ocean under the continental fragment would have resulted in a synclinal "V" shaped continental block between Laurentia and Iapetus. From Karabinos et al. (1998).

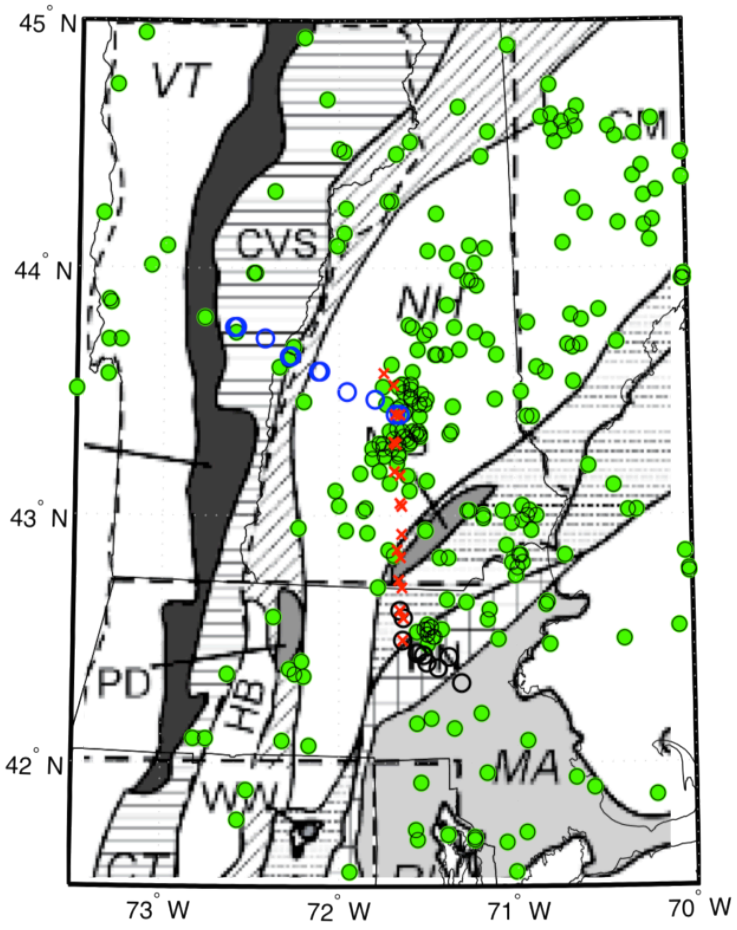

Figure 12. Moho Ps conversion points from Figure 8 and earthquake epicenters (green dots) from figure 2. Notice the central New Hampshire seismicity cluster near the intersection of transect 1 (blue circles) and transect 2 (red X's). The seismicity cluster laterally coincides with the location of "H1 offset A" and a change in crustal thickness that is observed in Figure 10 on transect 2.

The transition from Transect 1 to Transect 2 on Figure 10 occurs near the center of the CMB where a prominent seismicity cluster is observed in central New Hampshire (Figure 12). The H1 crustal horizon in the CMB is interpreted to be offset in this area ("H1 offset A" in Figure 10), near the intersection of Transect 1 with Transect 2. Both the "H1 offset A" observed

in this study and the central New Hampshire seismicity cluster occur just east of a proposed surface location for the principle Iapetan suture in New England, a.k.a. the Red Indian Line thrust-fault ("RILa" in Figure 13). If the location of "H1 offset A" were projected to the location of RILa in Figure 13, it would suggest a fault that dips roughly to the east. An eastward-dipping earthquake source fault for the earthquakes in central New Hampshire is supported by focal mechanisms and earthquake-location analysis (Starr, 2013). "H1 offset A" in Figure 10 may be an observed offset between Ganderian crust and the remnant subducted Iapetus Ocean crust that would have been pinned between the Laurentian margin and Ganderia during continent-continent collision.

If the location of "H1 offset A" in Figure 10 is a contact between Ganderian and Iapetan crust related to the Red Indian Line thrust fault, then present day seismicity in central New Hampshire (which has been attributed to an after-shock sequence of a magnitude 6.5 earthquake in 1638 (Ebel et al., 2000)) might be related to stress-release along the principal Iapetan suture. Most of the earthquakes in this area occur in the relatively shallow 3-10 km depth range with an average reported focal depth error of ±7.5 km (Ebel and Kafka, 1991). If the "H1 offset A" observed at the 10-20 km depth range in Figure 10 is an observed offset related to RILa in Figure 13, then the seismicity cluster in Central New Hampshire shows some spatial correlation with the RILa thrust fault. However, tighter constraints of earthquake focal depth and higher resolution crustal imaging surveys are required to verify the source fault for earthquakes in central New Hampshire.

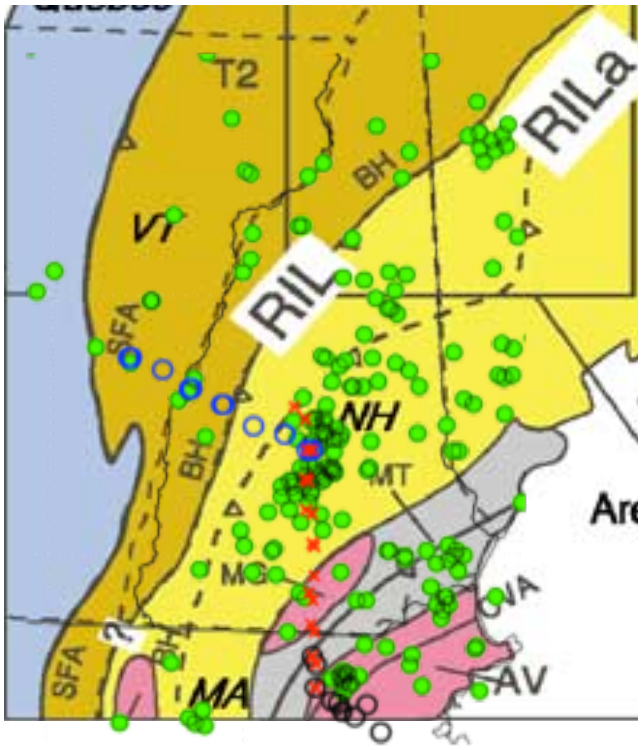

Figure 13. Ps conversion points from Figure 8 overlaying a map of northern New England terranes, sutures, and tectonic features from Moench and Aleinikoff (2003). The location of the Red Indian Line (RIL) on the map is in question as indicated by the two southeast dipping thrust faults labeled as "RIL" and "RILa" (the "a" stands for alternate). "H1 offset A" occurs just east of RILa and might be related to the principal Iapetan suture.

Moving south on Transect 2 on Figure 10, the Moho remains apparently flat until south of the CMB-Merrimack terrane boundary where Moho depth increases and the H1 crustal horizon is again interpreted to be offset ("H1 offset B" in Figure 10). At this point, both the Moho and crustal horizon take on an apparent northerly dip. This apparent northerly dip may be associated with the Clinton-Newbury fault, which bounds the PN and Merrimack terranes and has been shown to plunge under the Merrimack terrane (Fisk, 1985). If "H1 offset B" (Figure 10) under the Merrimack terrane is indeed related to the boundary between Merrimack and PN terranes, then much of the PN terrane may be underthrust beneath the Merrimack terrane, a

characteristic that is also consistent with computer modeling of gravity data from Fisk (1985). There are no crustal structures interpreted in the Figure 10 cross-section that correlate with the CMB-Merrimack terrane boundary.

The transition from Transect 2 to Transect 3 on Figure 10 occurs very close to the Merrimack-PN border. The major feature interpreted in Transect 3 is an apparent offset of both the Moho and the H1 crustal horizon ("H1 offset C") under the PN terrane. This offset is interpreted here as the west dipping Bloody Bluff fault which bounds the PN and Avalon terranes. Geologic mapping of the Bloody Bluff fault has indicated that the fault is west/northwest dipping (Goldsmith, 1991), which is consistent the Bloody Bluff fault dip interpreted in this study. Hepburn (2006) suggests that the PN terrane was the overriding plate during subduction of either the Merrimack terrane, the Avalon terrane, or both. Considering the apparent northwest-dipping H1 crustal horizon and Moho offset beneath the PN terrane as well as the interpreted dip of the Clinton-Newbury and Bloody Bluff faults, there appears to be structural evidence for thrusting of the PN slab under the Merrimack slab and thrusting of the Avalon slab under the PN slab.

5. DISCUSSION

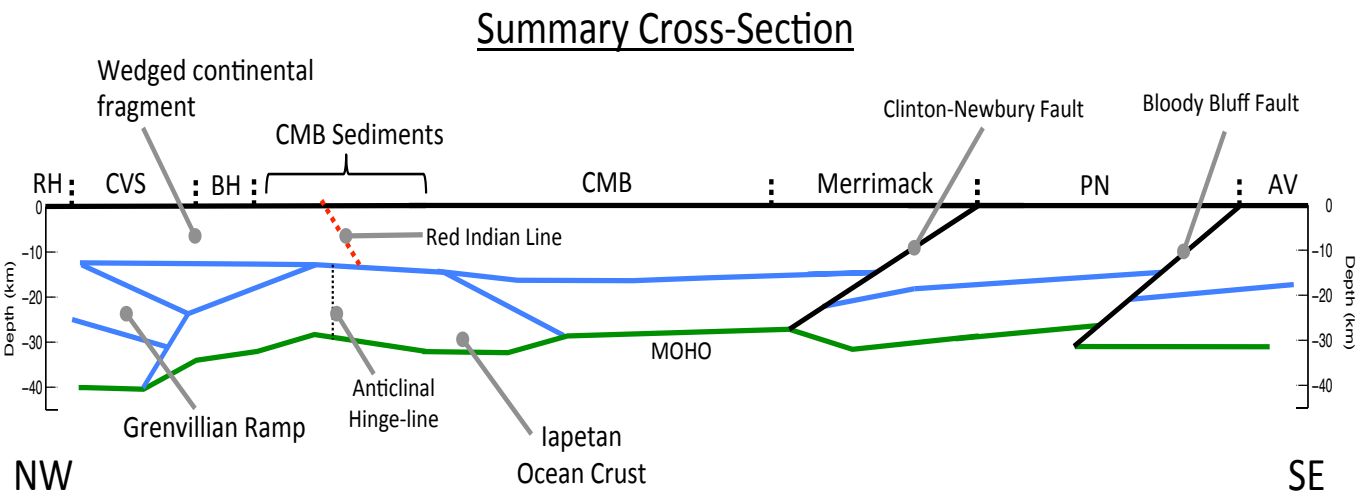

Figure 14. Cross-section summarizing the crustal structure of the New England tectonostratigraphic terranes as interpreted from Section 4. Blue lines are crustal layers as inferred from the PcS conversion points in Figures 9 and 10. Green line is the Moho as inferred from PmS conversion points in Figures 9 and 10. The Summary cross-section runs approximately southeast (SE) from the Avalon terrane northwest (NW) to the Rowe Hawley terrane. See section 2.2 for terrane name abbreviations.

The interpreted receiver function data from Section 4 is organized into a summary cross-section of the New England tectonostratigraphic terranes in Figure 14. The summary cross-section is based on the observed receiver function data from Section 4 as well as numerous geologic studies that provide information on the crustal assemblage of the terranes (see Section 4). The Bloody Bluff Fault that forms the boundary between the Avalon terrane and the PN terrane is shown to dip to the west and cut through the entirety of the crust, as made evident by the offset of both the crustal horizon and Moho. The west dipping Bloody Bluff Fault is evidence of westerly thrusting of the Avalon terrane beneath the PN terrane. The Clinton-Newbury fault that bounds the PN and Merrimack terranes is also observed as a west-dipping fault in the Figure 14 cross-section. A crustal horizon offset and change in Moho depth correspond with the

projected location of the Clinton-Newbury fault, allowing the boundary between the PN and Merrimack to be resolved at depth. This westerly dip of the Clinton-Newbury is evidence for thrusting of the PN terrane beneath Ganderia (the CMB and Merrimack terranes).

No crustal structures are observed at depth in this study that correspond with the Merrimack-CMB terrane boundary. The lack of structural evidence observed in this study to distinguish the Merrimack terrane from the CMB terrane is not surprising because receiver functions are a relatively low resolution seismic method and CMB and Merrimack terranes are expected to be built upon the same Ganderian continental basement (van Staal, 2009) and differentiated primarily by a change in continental sediment derivation at the surface (Hussey et al., 2010; Dorais et al., 2009).

The western boundary of Ganderia is the Red Indian Line in Figure 14. Several authors (e.g. van Staal, 1998; Dorais and Paige, 2000; Moench and Aleinikoff, 2003) discuss difficulties placing the location of the Red Indian Line, which is considered the principal Iapetan suture in the Northern Appalachians. The purpose of the Red Indian Line is to designate all terranes situated to the west of the line as those originating from the Laurentian side of the Iapetus while all terranes to the east of the line are derived from the Gondwanan side of the Iapetus (Dorais et al., 2012). The Red Indian Line has been placed in multiple locations in New England e.g., the eastern border of the CVS (van Staal, 1998), the eastern border of the Bronson Hill terrane (e.g., Moench and Aleinikoff, 2003), and buried under Central Maine trough sediments east of the BH-CMB surficial terrane boundary (Dorais and Paige, 2000; Moench and Aleinikoff, 2003). The Red Indian Line (RIL) in this study is placed above the anticlinal hinge-line of the remnant subducted-slab of the Iapetus Ocean in Figure 14 that was interpreted from the data in Section 4. The anticlinal shape of the remnant Iapetan slab is indicative of an oceanic plate that experienced

dual subduction polarity (Figure 15) where the oceanic crust was subducted under both Laurentia that is located to the west of the RIL (Karabinos et al., 1998) and Ganderia that is located to the east of the RIL (Moench and Aleinikoff, 2003). If the RIL is to represent the location where the Iapetus Ocean closed, then the RIL should be placed approximately above the remnant oceanic slab's anticlinal hinge-line because this location is where continental crust on opposite sides of a dual-subduction-polarity zone would collide. The Red Indian Line is projected to the surface above the anticlinal hinge-line with dip-direction supported by Dorais and Paige (2000) and Moench and Aleinikoff (2003). This RIL location is also consistent with the Red Indian Line location proposed by Dorais and Paige (2000) and Moench and Aleinikoff (2003), who leave the Iapetan suture buried by CMB sediments.

In Figure 14, the Red Indian Line separates Ganderia from a continental fragment that became wedged between Laurentia and Ganderia during the closure of the Neo-Iapetus and Iapetus Oceans (Karabinos et al., 1998). The "V" shaped crustal horizon of the continental fragment is evidence for easterly subduction of the Neo-Iapetus beneath the crustal fragment, which formed the Shelburne Falls Arc (now located on the western edge of the CVS and east of the RH), and westerly subduction of the Iapetus beneath the crustal fragment, which formed the Bronson Hill Arc (Karabinos et al., 1998). The western edge of the Appalachian lithologies terminates along the Grenvillian ramp (Hughes and Luetgert, 1991) shown in Figure 14, which dips to the east underneath the CVS and RH.

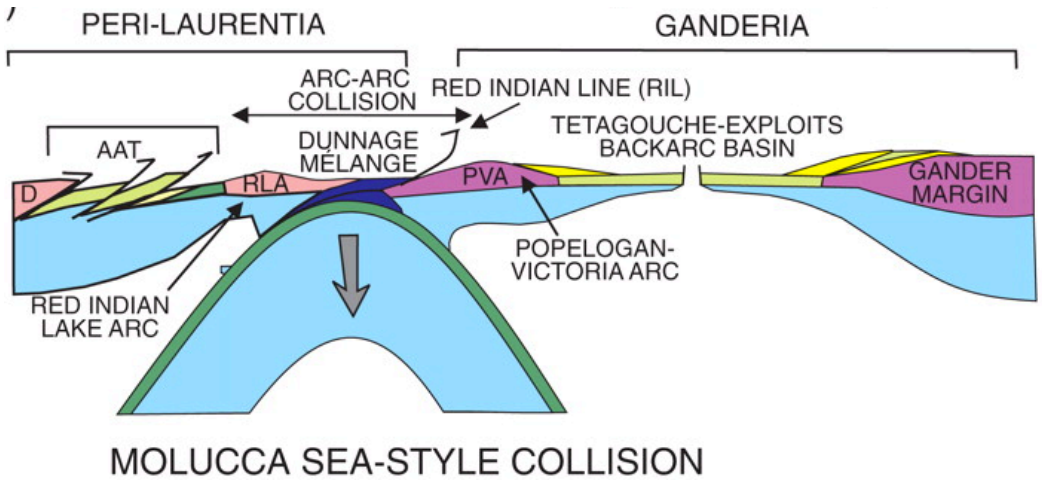

Figure 15. Example of dual oceanic subduction polarity that the Iapetus Ocean is proposed to have experienced. From van Staal (2009).

6. CONCLUSIONS

Receiver functions created from a line of 17 broadband seismic stations in New England were used to decipher lateral changes in seismic velocity structure associated with the tectonostratigraphic terranes from central Vermont to eastern Massachusetts. The receiver functions were capable of detecting the Moho and as many as three mid-crustal horizons within the study area. Crustal thickness along the line of stations was found to be greatest in the west and showed an irregular thinning toward the east. On the northwestern edge of the study area, an east-dipping, mid-crustal ramp is observed that is interpreted here as the boundary between Grenvillian and Appalachian lithologies. This ramp structure is consistent with the findings of the Hughes and Luetgert (1991) seismic refraction/ reflection study. The easterly dip of the Grenvillian ramp suggests thrusting of the western margin of the Appalachians over Laurentia (Grenville) and is consistent with the tectonic model of Karabinos et al. (1998).

The RH, CVS, and BH terranes are built on a continental fragment that exhibits a synclinal "V" shaped profile within the mid-crust. The synclinal "V" shape of the mid-crustal horizon indicates a continental fragment that experienced thrusting over both its bounding continental bodies (Laurentia to the west and Ganderia to the east). The western side of this continental fragment is interpreted to have been thrust over the Laurentian margin during easterly subduction of the Neo-Iapetus Ocean while the eastern side of the continental fragment appears to have been thrust over the Ganderian margin during westerly subduction of the Iapetus Ocean (Karabinos et al., 1998).

A remnant portion of the subducted Iapetan oceanic crust is interpreted in this study to reside beneath the BH terrane and western portion of the CMB. The remnant oceanic slab exhibits an anticlinal shape whose hinge line coincides with the Red Indian Line location as interpreted by Dorais and Paige (2000) and Moench and Aleinikoff (2003). The RIL (principal Iapetan suture) divides crust of Laurentian affinity from crust of Gondwanan affinity, but also denotes the present-day location of the closure of the Iapetus Ocean. If the Iapetus Ocean experienced dual subduction polarity between Laurentia and Ganderia (Figure 15) as proposed by van Staal (2009), then the Iapetan suture (Red Indian Line) should be located above the anticlinal hinge-line of the remnant Iapetan ocean crust, where continental crust on opposite sides of a dual-subduction-polarity zone would have collided. Thus, the location of the Red Indian Line in this study is placed just east of the BH-CMB terrane boundary based on the location of the anticlinal hinge-line of the remnant Iapetan Ocean crust shown in Figure 14, which is where crust of Laurentian affinity would have met crust of Gondwanan affinity upon the closing of the Iapetus Ocean.

The receiver function results of this thesis suggest an offset within the mid-crust located just to the west of the PN-Merrimack surficial terrane boundary. This mid-crustal offset is evidence of crustal faulting. Just west of the aforementioned offset, a shallowing of Moho depth is observed in the receiver function results. Shallowing of Moho depth could indicate uplift of this portion of the crust relative to the surrounding crust. The mid-crustal faulting in conjunction with a relatively abrupt shallowing of the Moho depth on the west side of the fault is considered here to be evidence for a west-dipping Clinton-Newbury fault, indicating thrusting of Ganderia over the PN terrane.

An abrupt and concurrent offset of both the Moho and the mid-crustal horizon is interpreted under the PN terrane. This offset is interpreted as the deep extension of the Bloody Bluff Fault, which bounds the Avalon and Nashoba terranes. Dip direction of the fault suggests thrusting of the PN terrane over the Avalon terrane.

"H1 offset A" in Figure 10 is interpreted in this study to be a crustal offset between Ganderian crust and the remnant Iapetan oceanic slab. The offset roughly coincides with the proposed surface location of the principle Iapetan suture (the east dipping Red Indian Line thrust fault) from Moench and Aleinikoff (2003) and is interpreted here as an offset between Ganderian crust and the remnant subducted Iapetus Ocean slab. Of the several crustal offsets observed in this study that are associated with known faults or crustal sutures, only the Red Indian Line thrust fault has a spatial correspondence with a cluster of seismicity in the region. But higher resolution images of the mid crust in central New Hampshire are needed to confirm the offset observed in this study and to relate the earthquakes in that area to this possible structure in the middle and lower crust.

References

Ammon CJ. 1991. The isolation of receiver effects from teleseismic P waveforms. Bulletin of the Seismological Society of America 81: no. 6, 2594-2510.

Ammon CJ. 1997. An Overview of Receiver Function Analysis. http://eqseis.geosc.psu.edu/~cammon/HTML/RftnDocs/rftn01.html

Ando CJ, Czuchra BL, Klemperer SL, Brown LD, Cheadle MJ, Cook FA, Oliver JE, Kaufman S, Walsh T, Thompson Jr JB, Lyons JB, Rosenfeld JL. 1984. Crustal Profile of Mountain Belt: COCORP Deep Seismic Reflection Profiling in New England Appalachians and Implications for Architecture of Convergent Mountain Chains. The American Association of Petroleum Geologists Bulletin 68: 819-837.

Bell KG. 1968. Faults in eastern Massachusetts. Geological Society of America Special Paper 115: 250.

Coish RA. 2010. Magmatism in the Vermont Appalachians. The Geological Society of America, Memoir 206: 91-110.

Diaconescu CC, Knapp JH, Brown LD, Steer DN, and Stiller M. 1998. Precambrian Moho Offset and Tectonic Stability of the East European Platform from the URSEIS Deep Seismic Profile. Geology 26: 211-214

Di Stefano R, Bianchi I, Ciaccio MG, Carrara G, and Kissling E. 2011.Three−dimensional Moho topography in Italy: New constraints from receiver functions and controlled source seismology. Geochemistry Geophysics Geosystems 12.

Doll WH, Domoracki WJ, Costain JK, Coruh C, Ludman A, and Hopeck JT. 1996. Seismic reflection evidence for the evolution of a transcurrent fault system; the Norumbega fault zone, Maine. Geology 24: 251-254.

Dorais MJ and Paige ML. 2000. Regional geochemical and isotopic variations of northern New England plutons: Implications for magma sources and for Grenville and Avalon basement-terrane boundaries. Geological Society of America Bulletin 112: 900-914

Dorais MJ, Wintsch RP, Nelson WR, and Tubrett M. 2009. Insights into the Acadian orogeny, New England Appalachians: a provenance study of the Carrabassettt and Kittey formations, Maine. Atlantic Geology 45: 50-71.

Ebel J. 2007. Results from 30 years of regional seismic network monitoring in New England. Abstracts with Programs. Geological Society of America 39: 35.

Ebel J, Bonjer KP, and Oncescu MC. 2000. Paleoseismicity: Seismicity evidence for past large earthquakes. Seismological Research Letters 71: 283-294.

Ebel J and Kafka AL. 1991. Earthquake activity in the Northeastern United States. The Geology of North America, Decade Map Volume 1: 227-290.

Eagar KC, Fouch MJ, and David JE. 2010. Receiver function imaging of upper mantle complexity beneath the Pacific Northwest, United States. Earth and Planetary Science Letters 297: 140-152.

Fisk PS. 1985. A Detailed Gravity Survey of the Clinton-Newbury and Wekepeke Faults in the Clinton, Massachusetts Area. MS Thesis. Boston College, Chestnut Hill, MA.

Foley JE. 1984. The crustal receiver structure beneath the Weston Observatory from long-period synthetic seismogram analysis. MS Thesis. Boston College, Chestnut Hill, MA.

Foley JE. 1990. Crustal Structure from Teleseismic Body Wave Data. PhD Dissertation. Massachusetts Institute of Technology, Cambridge, Massachusetts.

Gilbert H. 2012. Crustal Structure and Signatures of Recent Tectonism as Influenced by Ancient Terranes in the Western United States. Geosphere 8: 141-157.

Goldsmith R. 1991. Structural and Metamorphic History of Eastern Massachusetts. The Bedrock Geology of Massachusetts: US Geological Survey Professional Paper 1366-E-J: F1-F22.

Hatcher RD. 2010. The Appalachian orogen: A brief summary. The Geological Society of America, Memoir 206: 1-19.

Hepburn JC. 2006. Magmatism as guide to Siluro-Devonian tectonic settings of the Nashoba and Composite Avalon terranes in eastern Massachusetts. Abstracts with Programs. Geological Society of America 38: 33.

Hepburn JC, Dunning GR, and Hon R. 1995. Geochronology and regional tectonic implications of Silurian deformation in the Nashoba terrane, Southeast New England, USA. Current Perspectives in the Appalachian-Caledonian Orogen: Geological Association of Canada, Special Paper 41: 349-366.

Hughes S and Luetgert J. 1992. Crustal structure of the southeastern Grenville province, northern New York state and eastern Ontario. Journal of Geophysical Research 97(B12):17455-17.

Hussey AM, Bothner WA, and Aleinikoff J. 2010. The tectono-stratigraphic framework and evolution of southwestern Maine and southeastern New Hampshire. The Geological Society of America, Memoir 206: 205-230.

Karabinos P, Samson SD, Hepburn JC, and Stoll HM. 1998. Taconian Orogeny in the New England Appalachians: Collision between Laurentia and the Shlburne Falls arc. Geology 26: 215-218.

Kennett BLN. 2005. Seismological Tables: ak135. Research School of Earth Sciences at The Australian National University. Canberra ACT 0200. Australia.

Korsch RJ, Johstone DW, and Wake-Dyster KD.1997. Crustal architecture of the New England Orogen based on deep seismic reflection profiling. In: Tectonic and Metallogenesis of the New England Orogen, Geological Society of Australia Special Publication 19, 29-51.

Kusznir NJ, and Matthews DH. 1988. Deep reflections and the deformational mechanics of the continental lithosphere. Journal of Petrology, Special Lithosphere Issue: 63–87.

Langston CA. 1979. Structure under Mount Rainier, Washington, inferred from teleseismic body waves. Journal of Geophysical Research 84(B9):4749-62.

Levander A. 2003. USArray Design Implications for Wavefield Imaging in the Lithosphere. The Leading Edge 22. 250-255.

Li A, Fischer KM, van der Lee S, and Wysession ME. 2002. Crust and upper mantle discontinuity structure beneath eastern North America. Journal of Geophysical Research 107(B5).

Ligorria JP and Ammon C. 1999. Iterative deconvolution and receiver-function estimation. Bulletin of the Seismological Society of America 89: 1395-1400.

Moench RH and Aleinikoff JN. 2003. Stratigraphy, geochronology, and accretionary terrane settings of two Bronson Hill arc sequences, northern New England. Physics and Chemistry of the Earth 28: 113-160.

Mohsen A. 2004. A Receiver Function Study of the Crust and Upper Mantle Across the Dead Sea Transform. PhD Dissertation. Free University of Berlin, Berlin, Germany.

Sheriff RE and Geldart LP. 1995. *Exploration Seismology*. Cambridge University Press ©1995. New York.

Skehan JW. 1969. Tectonic framework of Southern New England and Eastern New York. North Atlantic-Geology and continental drift; A symposium. American Association of Petroleum Geologists Memoir 12: 793-814.

Starr JC. 2013. A Geophysical and Field Survey in Central New Hampshire to Search for the Source Region of the Magnitude 6.5 Earthquake of 1638. MS Thesis. Boston College, Chestnut Hill, MA.

Stein S and Wysession M. *An Introduction to Seismology, Earthquakes, and Earth Structure*. Blackwell Publishing ©2003. 350 Main Street, Malden, MA 02148-5020, USA.

Stroud MM. 2007. Temporal and Directional Constraints on a Major Shear Zone in Eastern Massachusetts. MS Thesis. Boston College, Chestnut Hill, MA.

Taylor SR and Toksoz MN. 1979. Thre-Dimensional Crust and Upper Mantle Structure of the Northeastern United States. Journal of Geophysical Research 84: 7627:7644.

van Staal CR, Dewey JF, Mac Niocaill C, KcKerrow, WS. 1998. The Cambrian–Silurian tectonic evolution of the northern Appalachians and British Coledonides: history of a complex, west and southwest Pacific-type segment of Iapetus. In Lyell: The past is the key to the present. Edited by D.J. Blundell and A.C. Scott. Geological Society of London, Special Publications 143. pp. 199– 242.

van Staal CR, Whalen JB, Pablo VV, Zagorevski A, and Rogers N. 2009. Pre-Carboniferous, episodic accretion-related, orogenesis along the Laurentian margin of the northern Appalachians. Geological Society of London, Special publication; 327:271-316.

Yamauchi M, Hirahara K, Shibutani T. 2003. High resolution receiver function imaging of the seismic velocity discontinuities in the crust and the uppermost mantle beneath southwest Japan. Earth Planet Science 55: 59-64.

Zen E, Hepburn JC, Kidd WSF, Robinson P, Skehan JW, and Tompson JB.1989. *Tectonostratigraphic Terranes in the Nothern Appalachians: Their Distribution, Origin, and Age; Evidence for Their Existance*. American Geophysical Union © 1989. 2000 Florida Ave., N.W. Washington, D.C. 20009.

ZHU C. 1996. Crustal thickness Across the Grenville Province and Northern Appalachians in New England and Adjacent Areas. MS Thesis. Boston College, Chestnut Hill, Massachusetts.

Zhu H and Ebel J. 1994. Tomographic inversion for the seismic velocity structure beneath northern New England using seismic refraction data. Journal of Geophysical Research 99(B8):15331-15.

Appendix 1: Ray Parameter and Receiver Function Moveout

Appendix 1.1: Ray Parameter

The ray parameter, also known as the horizontal slowness, is a constant value determined by a ray path's initial angle of incidence as it moves outward from a seismic source (Figure A1). The depth and distance of a source relative to a particular seismic station will determine the theoretical ray parameter (Table 1) at any given seismic station. In general, the farther away and deeper an event is from a particular seismic station, the lower its ray parameter and the more steeply (or vertically) the ray will approach the seismic station. The ray parameter is determined using Snell's Law and can be used to group receiver functions for stacking. Events with a similar ray parameter and BAZ will sample similar structures under a seismic station and cause the receiver function conversions and multiples to align. Events with a different ray parameter will have conversions and multiples that arrive out of phase (Figure A3) for a given velocity structure.

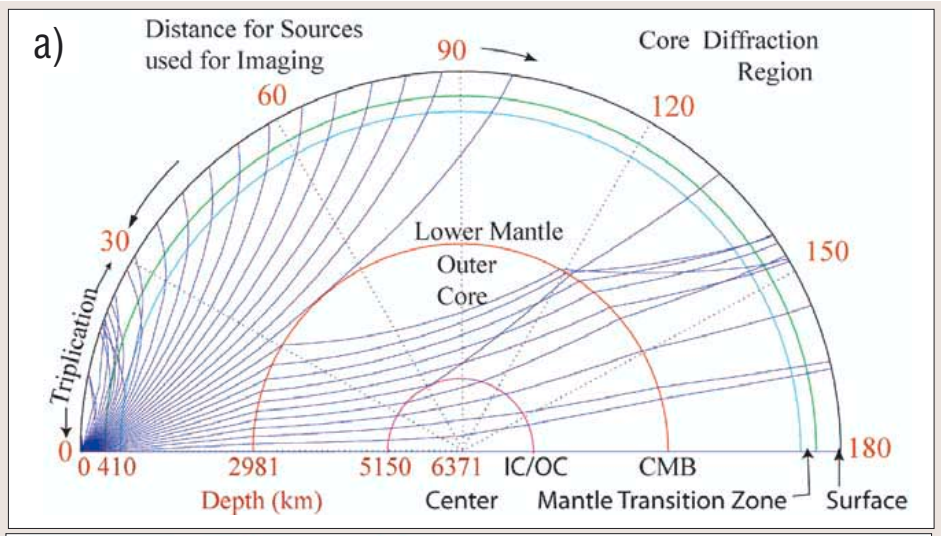

Figure A1. Illustration of how ray paths travel outward from a seismic source in the earth (from Levander, 2003). Rays will refract according to Snell's Law. The ray parameter (horizontal slowness) is constant along each ray and will predict the angle at which a seismic ray approaches a receiver based on the depth of the source and the distance between the source and receiver.

Depth (km)	Delta(°)	0.00	15.00	35.00	50.00	100.00	150.00	200.00	250.00	300.00	350.00	400.00	450.00	500.00	550.00	600.00	650.00	700.00
	30.00	0.080	0.080	0.080	0.080	0.079	0.079	0.079	0.079	0.079	0.079	0.078	0.078	0.078	0.077	0.077	0.077	0.08
	31.00	0.079	0.079	0.079	0.079	0.079	0.079	0.079	0.079	0.079	0.078	0.078	0.078	0.077	0.077	0.077	0.076	0.08
	32.00	0.079	0.079	0.079	0.079	0.079	0.079	0.078	0.078	0.078	0.078	0.077	0.077	0.077	0.076	0.076	0.076	0.08
	33.00	0.079	0.079	0.079	0.079	0.078	0.078	0.078	0.078	0.077	0.077	0.077	0.077	0.076	0.076	0.076	0.075	0.07
	34.00	0.078	0.078	0.078	0.078	0.078	0.078	0.077	0.077	0.077	0.077	0.076	0.076	0.076	0.075	0.075	0.075	0.07
	35.00	0.078	0.078	0.078	0.077	0.077	0.077	0.077	0.077	0.076	0.076	0.076	0.076	0.075	0.075	0.074	0.074	0.07
	36.00	0.077	0.077	0.077	0.077	0.077	0.077	0.076	0.076	0.076	0.076	0.075	0.075	0.075	0.074	0.074	0.074	0.07
	37.00	0.077	0.076	0.076	0.076	0.076	0.076	0.076	0.075	0.075	0.075	0.075	0.074	0.074	0.074	0.073	0.073	0.07
	38.00	0.076	0.076	0.076	0.076	0.076	0.075	0.075	0.075	0.075	0.074	0.074	0.074	0.074	0.073	0.073	0.072	0.07
	39.00	0.075	0.075	0.075	0.075	0.075	0.075	0.075	0.074	0.074	0.074	0.074	0.073	0.073	0.073	0.072	0.072	0.07
	40.00	0.075	0.075	0.075	0.075	0.074	0.074	0.074	0.074	0.073	0.073	0.073	0.073	0.072	0.072	0.072	0.071	0.07
	41.00	0.074	0.074	0.074	0.074	0.074	0.074	0.073	0.073	0.073	0.073	0.072	0.072	0.072	0.071	0.071	0.071	0.07
	42.00	0.074	0.074	0.073	0.073	0.073	0.073	0.073	0.073	0.072	0.072	0.072	0.071	0.071	0.071	0.070	0.070	0.07
	43.00	0.073	0.073	0.073	0.073	0.073	0.072	0.072	0.072	0.072	0.071	0.071	0.071	0.070	0.070	0.070	0.069	0.07
	44.00	0.072	0.072	0.072	0.072	0.072	0.072	0.071	0.071	0.071	0.071	0.070	0.070	0.070	0.070	0.069	0.069	0.07
	45.00	0.072	0.072	0.072	0.071	0.071	0.071	0.071	0.071	0.070	0.070	0.070	0.070	0.069	0.069	0.069	0.068	0.07
	46.00	0.071	0.071	0.071	0.071	0.071	0.070	0.070	0.070	0.070	0.069	0.069	0.069	0.069	0.068	0.068	0.068	0.07
	47.00	0.070	0.070	0.070	0.070	0.070	0.070	0.070	0.069	0.069	0.069	0.069	0.068	0.068	0.068	0.067	0.067	0.07
	48.00	0.070	0.070	0.070	0.070	0.069	0.069	0.069	0.069	0.068	0.068	0.068	0.068	0.067	0.067	0.067	0.066	0.07
	49.00	0.069	0.069	0.069	0.069	0.069	0.068	0.068	0.068	0.068	0.068	0.067	0.067	0.067	0.066	0.066	0.066	0.07
	50.00	0.068	0.068	0.068	0.068	0.068	0.068	0.068	0.067	0.067	0.067	0.067	0.066	0.066	0.066	0.066	0.065	0.06
	51.00	0.068	0.068	0.068	0.068	0.067	0.067	0.067	0.067	0.066	0.066	0.066	0.066	0.066	0.065	0.065	0.065	0.06
	52.00	0.067	0.067	0.067	0.067	0.067	0.066	0.066	0.066	0.066	0.066	0.065	0.065	0.065	0.065	0.064	0.064	0.06
	53.00	0.066	0.066	0.066	0.066	0.066	0.066	0.066	0.066	0.065	0.065	0.065	0.065	0.064	0.064	0.064	0.063	0.06
	54.00	0.066	0.066	0.066	0.066	0.065	0.065	0.065	0.065	0.065	0.064	0.064	0.064	0.064	0.063	0.063	0.063	0.06
	55.00	0.065	0.065	0.065	0.065	0.065	0.065	0.064	0.064	0.064	0.064	0.064	0.063	0.063	0.063	0.062	0.062	0.06
	56.00	0.064	0.064	0.064	0.064	0.064	0.064	0.064	0.064	0.063	0.063	0.063	0.063	0.062	0.062	0.062	0.062	0.06
	57.00	0.064	0.064	0.064	0.064	0.063	0.063	0.063	0.063	0.063	0.062	0.062	0.062	0.062	0.061	0.061	0.061	0.06
	58.00	0.063	0.063	0.063	0.063	0.063	0.063	0.062	0.062	0.062	0.062	0.062	0.061	0.061	0.061	0.061	0.060	0.06
	59.00	0.062	0.062	0.062	0.062	0.062	0.062	0.062	0.062	0.061	0.061	0.061	0.061	0.060	0.060	0.060	0.060	0.06
	60.00	0.062	0.062	0.062	0.062	0.061	0.061	0.061	0.061	0.061	0.061	0.060	0.060	0.060	0.060	0.059	0.059	0.06
	61.00	0.061	0.061	0.061	0.061	0.061	0.061	0.060	0.060	0.060	0.060	0.060	0.059	0.059	0.059	0.059	0.058	0.06
	62.00	0.060	0.060	0.060	0.060	0.060	0.060	0.060	0.060	0.059	0.059	0.059	0.059	0.059	0.058	0.058	0.058	0.06
	63.00	0.060	0.060	0.060	0.060	0.060	0.059	0.059	0.059	0.059	0.059	0.058	0.058	0.058	0.058	0.058	0.057	0.06
	64.00	0.059	0.059	0.059	0.059	0.059	0.059	0.059	0.058	0.058	0.058	0.058	0.058	0.057	0.057	0.057	0.057	0.06
	65.00	0.059	0.058	0.058	0.058	0.058	0.058	0.058	0.058	0.058	0.057	0.057	0.057	0.057	0.057	0.056	0.056	0.06
	66.00	0.058	0.058	0.058	0.058	0.058	0.058	0.057	0.057	0.057	0.057	0.057	0.056	0.056	0.056	0.056	0.055	0.06
	67.00	0.057	0.057	0.057	0.057	0.057	0.057	0.057	0.057	0.056	0.056	0.056	0.056	0.056	0.055	0.055	0.055	0.05
	68.00	0.057	0.057	0.057	0.057	0.056	0.056	0.056	0.056	0.056	0.056	0.055	0.055	0.055	0.055	0.054	0.054	0.05
	69.00	0.056	0.056	0.056	0.056	0.056	0.056	0.055	0.055	0.055	0.055	0.055	0.054	0.054	0.054	0.054	0.054	0.05
	70.00	0.055	0.055	0.055	0.055	0.055	0.055	0.055	0.055	0.054	0.054	0.054	0.054	0.054	0.053	0.053	0.053	0.05
	71.00	0.055	0.055	0.055	0.055	0.054	0.054	0.054	0.054	0.054	0.054	0.053	0.053	0.053	0.053	0.053	0.052	0.05
	72.00	0.054	0.054	0.054	0.054	0.054	0.054	0.053	0.053	0.053	0.053	0.053	0.053	0.052	0.052	0.052	0.052	0.05
	73.00	0.053	0.053	0.053	0.053	0.053	0.053	0.053	0.053	0.052	0.052	0.052	0.052	0.052	0.051	0.051	0.051	0.05
	74.00	0.053	0.053	0.053	0.053	0.052	0.052	0.052	0.052	0.052	0.052	0.051	0.051	0.051	0.051	0.051	0.050	0.05
	75.00	0.052	0.052	0.052	0.052	0.052	0.052	0.051	0.051	0.051	0.051	0.051	0.051	0.050	0.050	0.050	0.050	0.05
	76.00	0.051	0.051	0.051	0.051	0.051	0.051	0.051	0.051	0.050	0.050	0.050	0.050	0.050	0.050	0.049	0.049	0.05
	77.00	0.051	0.051	0.051	0.051	0.050	0.050	0.050	0.050	0.050	0.050	0.050	0.049	0.049	0.049	0.049	0.049	0.05
	78.00	0.050	0.050	0.050	0.050	0.050	0.050	0.049	0.049	0.049	0.049	0.049	0.049	0.049	0.048	0.048	0.048	0.05
	79.00	0.049	0.049	0.049	0.049	0.049	0.049	0.049	0.049	0.049	0.048	0.048	0.048	0.048	0.048	0.048	0.047	0.05
	80.00	0.049	0.049	0.049	0.049	0.048	0.048	0.048	0.048	0.048	0.048	0.048	0.047	0.047	0.047	0.047	0.047	0.05
	81.00	0.048	0.048	0.048	0.048	0.048	0.048	0.048	0.047	0.047	0.047	0.047	0.047	0.047	0.046	0.046	0.046	0.05
	82.00	0.047	0.047	0.047	0.047	0.047	0.047	0.047	0.047	0.047	0.046	0.046	0.046	0.046	0.046	0.045	0.045	0.05
	83.00	0.047	0.047	0.047	0.047	0.046	0.046	0.046	0.046	0.046	0.046	0.046	0.045	0.045	0.045	0.045	0.045	0.04
	84.00	0.046	0.046	0.046	0.046	0.046	0.046	0.045	0.045	0.045	0.045	0.045	0.045	0.045	0.044	0.044	0.044	0.04
	85.00	0.045	0.045	0.045	0.045	0.045	0.045	0.045	0.045	0.044	0.044	0.044	0.044	0.044	0.044	0.043	0.043	0.04
	86.00	0.045	0.044	0.044	0.044	0.044	0.044	0.044	0.044	0.044	0.044	0.043	0.043	0.043	0.043	0.042	0.042	0.04
	87.00	0.044	0.044	0.044	0.044	0.044	0.043	0.043	0.043	0.043	0.043	0.042	0.042	0.042	0.042	0.042	0.042	0.04
	88.00	0.043	0.043	0.043	0.043	0.043	0.042	0.042	0.042	0.042	0.042	0.042	0.042	0.042	0.042	0.042	0.042	0.04
	89.00	0.042	0.042	0.042	0.042	0.042	0.042	0.042	0.042	0.042	0.042	0.042	0.042	0.042	0.042	0.042	0.042	0.04
	90.00	0.042	0.042	0.042	0.042	0.042	0.042	0.042	0.042	0.042	0.042	0.042	0.042	0.042	0.042	0.042	0.042	0.04
	91.00	0.042	0.042	0.042	0.042	0.042	0.042	0.042	0.042	0.042	0.042	0.042	0.042	0.041	0.041	0.041	0.041	0.04
	92.00	0.042	0.042	0.042	0.042	0.042	0.042	0.042	0.041	0.041	0.041	0.041	0.041	0.041	0.041	0.041	0.041	0.04
	93.00	0.041	0.041	0.041	0.041	0.041	0.041	0.041	0.041	0.041	0.041	0.041	0.041	0.041	0.041	0.041	0.041	0.04
	94.00	0.041	0.041	0.041	0.041	0.041	0.041	0.041	0.041	0.041	0.041	0.041	0.041	0.041	0.041	0.041	0.041	0.04
	95.00	0.041	0.041	0.041	0.041	0.041	0.041	0.041	0.041	0.041	0.041	0.041	0.041	0.041	0.041	0.041	0.041	0.04

Table 1. Table of ray parameters (sec/km) for sources 0-95° away from a seismic station and for selected possible source depths. Modified from Kennett, 1995. The deeper and further the event is from a seismic station, the lower its ray parameter and thus the more vertical the ray path's angle of approach will be.

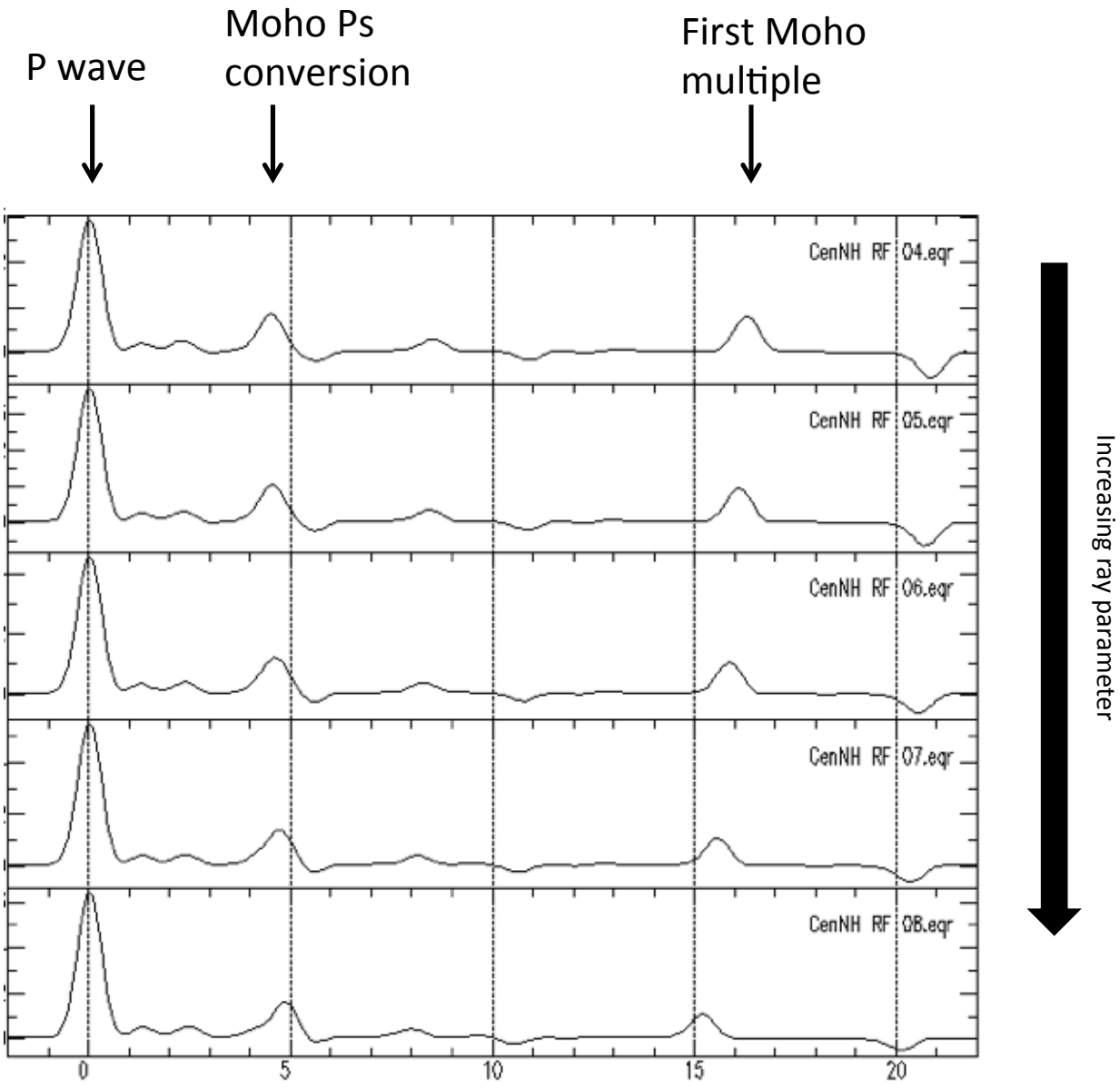

Figure A2. Synthetic receiver functions created from a 1D seismic velocity model for central New Hampshire. Each RF in the above figure was modeled after a source with a different ray parameter. The velocity model is held constant while ray parameter is changed from low to high (from top to bottom in figure). Notice how the direct Moho Ps conversion around 5 seconds (indicated by an arrow) moves further away in time from the P wave as ray parameter increases while the first Ps Moho multiple (also indicated by an arrow) moves closer in time to the P wave.

Appendix 1.2: Receiver Function Moveout Correction

The diagram below and subsequent equations explain how ray parameter affects the receiver function moveout and conversion point location under a seismic station.

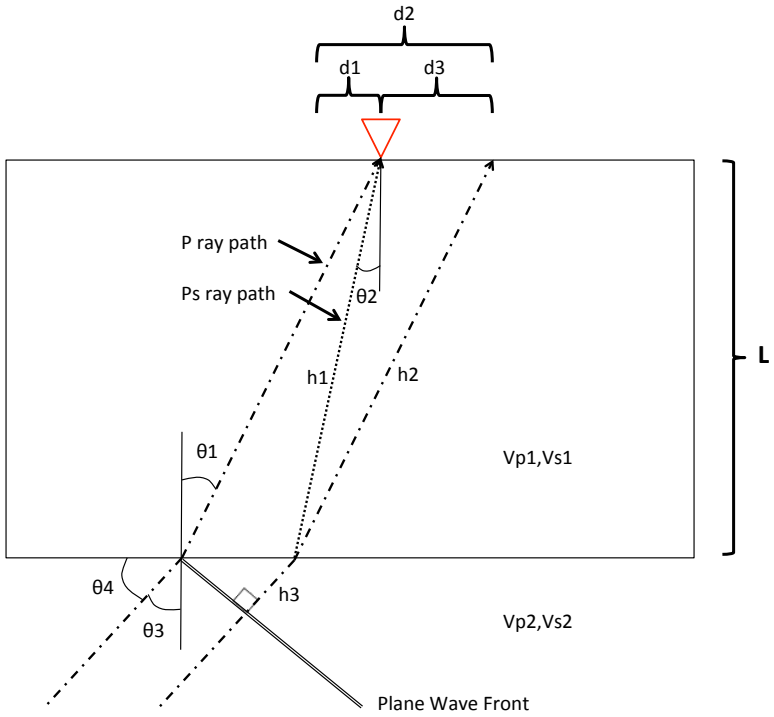

Figure A3. Diagram of Ps conversion moveout that relates ray parameter to Ps time delay (Td).

$p \equiv ray\ parameter \quad V \equiv velocity \quad VpX \equiv P\ wave\ velocity\ in\ Layer\ X$
$VsX \equiv S\ wave\ velocity\ in\ Layer\ X \quad L \equiv Thickness\ of\ top\ layer$
$d1 \equiv Horizontal\ distance\ between\ Ps\ conversion\ point\ and\ receiver$
$d3 \equiv Horizontal\ distance\ between\ P\ peircing\ point\ and\ receiver$

The following solves for the relationship between velocity model parameters and P-Ps arrival time difference (Td) that is needed for the moveout correction

$$p = {\sin\theta}/{V} \quad (definition\ of\ ray\ parameter\ (Horizontal\ Slowness))$$

$$\theta 1 = \sin^{-1}(p \cdot Vp1) \quad \theta 2 = \sin^{-1}(p \cdot Vs1) \quad \theta 3 = \sin(p \cdot Vp2) \quad \theta 4 = 90° - \theta 3$$

$$d1 = \tan(\theta 2) \cdot L \quad d2 = \tan(\theta 1) \cdot L \quad d3 = d2 - d1$$

$$h1 = \sqrt{L^2 + d1^2} \quad h2 = \sqrt{L^2 + d2^2} \quad h3 = \cos(\theta 4) \cdot d3$$

$$Td = \left({h3}/{Vp2} + {h1}/{Vs1}\right) - {h2}/{Vp1}$$

Appendix 2: Seismic Station Coordinates and Deployment Periods

Table 2. Table of seismic stations used in seismic array for this study. Locations and deployment periods are shown next to the station name.

Station	Latitude	Longitude	Deployment Start	Deployment End
S1	43.8229	-72.5993	July 8, 2011	November 1, 2011
S2	43.7783	-72.4280	March 15, 2012	August 20, 2012
HNH	43.7053	-72.2855	N/A	N/A
S3	43.6442	-72.1193	March 10, 2012	August 20, 2012
S4	43.5624	-71.9496	July 20, 2011	November 1, 2011
S5	43.5313	-71.8049	July 7, 2011	November 1, 2011
FFD	43.4701	-71.6533	N/A	N/A
S6	43.3517	-71.6448	June 20, 2012	November 2, 2012
S7	43.2323	-71.6414	June 20, 2012	November 2, 2012
S8	43.1065	-71.6188	July 29, 2012	November 2, 2012
S9	42.9811	-71.6102	June 20, 2012	November 2, 2012
S10	42.8710	-71.5869	January 25, 2012	May 20, 2012
S11	42.7488	-71.5789	January 20, 2012	May 20, 2012
S12	42.6257	-71.5715	January 20, 2012	May 20, 2012
HRV	42.5060	-71.5580	N/A	N/A
S13	42.4456	-71.4408	January 20, 2012	May 20, 2012
WES	42.3848	-71.3218	N/A	N/A

Appendix 3: Screening of Data for Final RF Analysis

The ideal dataset for any receiver function study would consist of hundreds of events recorded at each seismic station that is involved in the experiment. The ideal events would each have a high signal-to-noise ratio and the source locations would span a range of back azimuths and ray parameters. Likewise, stacking receiver functions requires multiple events of similar back azimuth and ray parameter if the researcher hopes to attain a detailed image of the receiver structure. Stacking of receiver functions from diverse back azimuths and ray parameters can be done, but only an averaged receiver structure will be obtained. Temporary receiver function arrays are typically in deployment for months to years and the researcher must usually work with data that are composed of only a handful of relatively low noise events. In general, large events that are close to the receiver are likely to have higher signal-to-noise ratios (SNR) when compared with events that are further away from the seismic station and/or have smaller magnitude.

This study analyzed all events of magnitude 5.7 or greater that occurred during the deployment period that were between 30°-95° from the seismic station. Magnitude 5.7 events are a typical minimum event size analyzed in receiver function studies (e.g., Li et al., 2002; Eager et al., 2010). Once all the possible receiver functions for a station were created (about 30 for the stations in this thesis), the data set was decreased to only those receiver functions which were considered to have pre-signal (pre P wave) noise that was lower than the post P wave signal (pre-signal noise is only available for analysis when the water-level deconvolution method is applied). This task reduced the dataset to 2-4 receiver functions for each temporary station. Examples of RFs from this study that contain different amounts of noise are shown in Figure A4.

There is no standard range for BAZ or RP that receiver functions should be grouped by for stacking. The acceptable range of BAZ or RP for stacking can only be determined by the researcher based on the goals of the study and/or observations made during the analysis.

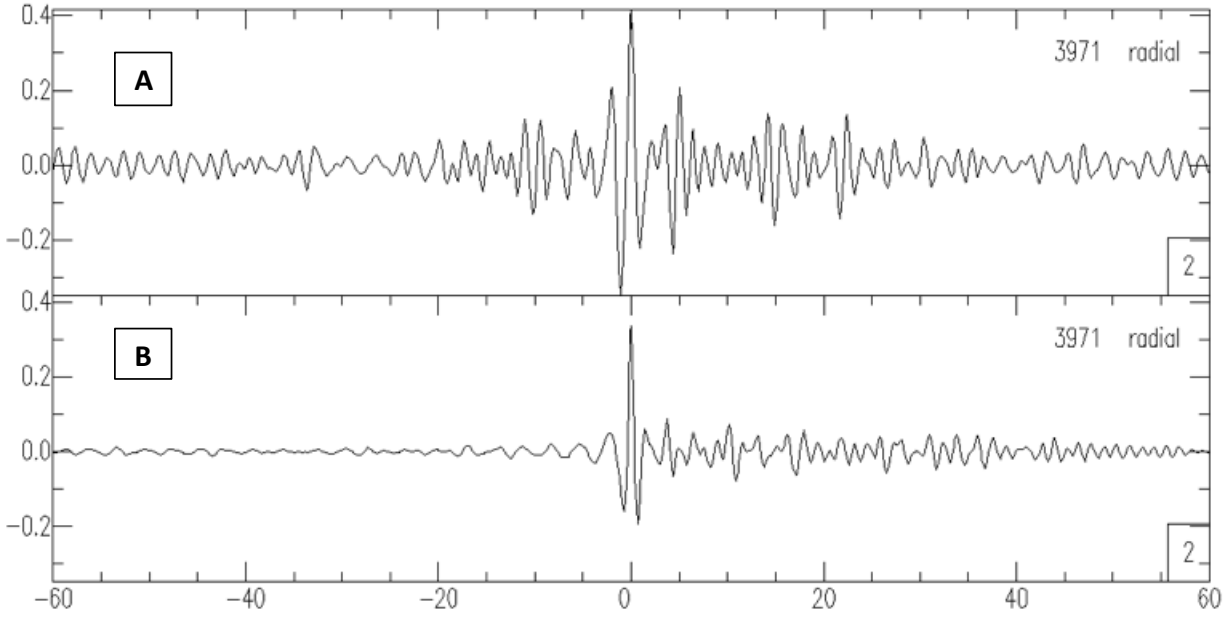

Figure A4. Example of receiver functions analyzed in this study that contain different amounts of noise. Receiver function 'A' is an example of a noisy receiver function that could be used if it can be stacked with other receiver functions. Receiver function 'B' is an example of a low-noise receiver function that could be interpreted on its own with no need to stack.

The purpose of this study was to decipher lateral changes in velocity structure from one terrane to the next. Detecting variations in structure of the terranes could require relatively high resolution imaging because of the lateral width of many of the terranes in question. A higher lateral resolution image of the crust is achievable in a receiver function study by grouping events into specific BAZ and RP bins. RFs created from sources of similar BAZ and RP will sample very similar structures. Through much trial and error, it was found that receiver functions used in

this study tended to have wave arrivals that were in phase when the events were in a BAZ and RP bin range of ±5° and ±0.05 sec/km, respectively. The relatively high SNR RFs that fell into this bin range were stacked. The final receiver function dataset is displayed with a ±22 second window around the P wave in Figure A5. Notice the low pre-signal noise before the P wave on all the RFs. Table 3 gives details on the events used in each receiver function that were analyzed in the final dataset. Many of the RFs used in the final analysis were not stacked because no other events within the stacking bin occurred during deployment.

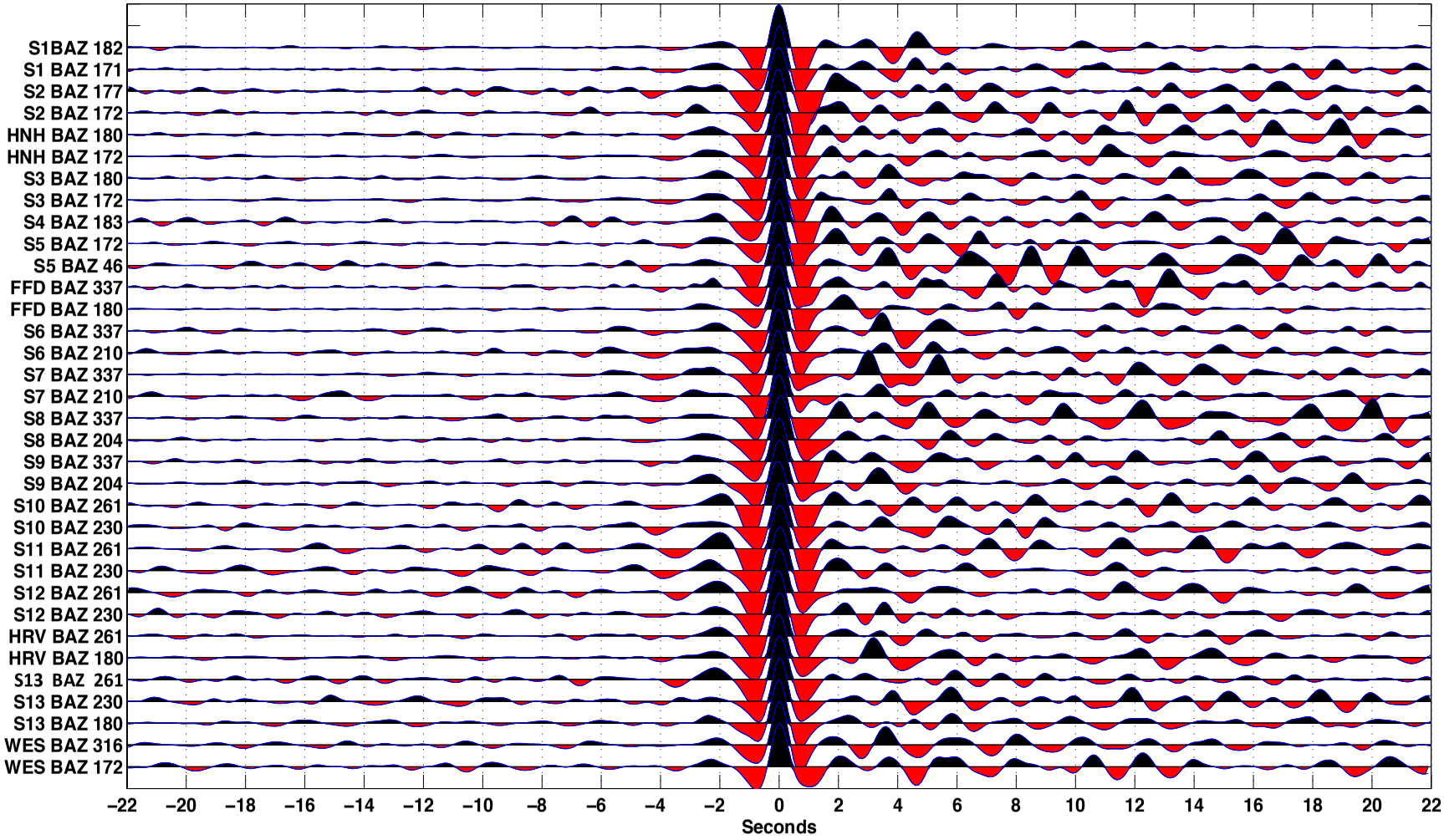

Figure A5. Final receiver function dataset with a ±22 second window around the P wave to show the influence seismic noise may have on the result. From top to bottom, RFs are plotted roughly from northwest to southeast. Station names with event BAZ are given on the left side of the figure.

Table 3. Source information for the events used in final receiver function dataset. Multiple events listed for one receiver function indicate that the events were stacked for the receiver function.

Receiver Function	Event Description								
	YearDay	YEAR	MONTH	DAY	ORIG TIME	LAT	LONG	DEPTH	MAG
S1 BAZ 182	236	2011	8	24	174611.65	-7.64	-74.53	147	7
S1 BAZ 171	245	2011	9	2	134709.64	-28.4	-63.07	577	6.7
S2 BAZ 177	135	2012	5	14	100040.23	-17.68	-69.59	105	6.2
S2 BAZ 172	149	2012	5	28	50723.45	-28.04	-63.09	586	6.7
HNH BAZ 180	70	2010	3	11	143943.95	-34.29	-71.89	11	6.9
	70	2010	3	11	145527.51	-34.33	-71.8	18	7
	85	2012	3	25	223706	-35.2	-72.22	40	7.1
	108	2012	4	17	35015.61	-32.62	-71.36	29	6.7
HNH BAZ 172	149	2012	5	28	50723.45	-28.04	-63.09	586	6.7
S3 BAZ 180	85	2012	3	25	223706	-35.2	-72.22	40	7.1
	108	2012	4	17	35015.61	-32.62	-71.36	29	6.7
S3 BAZ 172	149	2012	5	28	50723.45	-28.04	-63.09	586	6.7
S4 BAZ 183	236	2011	8	24	174611.65	-7.64	-74.53	147	7
	301	2011	10	28	185434.04	-14.44	-75.97	24	6.9
S5 BAZ 172	245	2011	9	2	134709.64	-28.4	-63.07	577	6.7
S5 BAZ 46	296	2011	10	23	104121	38.69	43.5	16	7.1
FFD BAZ 337	227	2012	8	14	25938.46	49.8	145.06	583	7.7
FFD BAZ 180	70	2010	3	11	143943.95	-34.29	-71.89	11	6.9
	70	2010	3	11	145527.51	-34.33	-71.8	18	7
	85	2012	3	25	223706	-35.2	-72.22	40	7.1
	108	2012	4	17	35015.61	-32.62	-71.36	29	6.7
S6 BAZ 337	227	2012	8	14	25938.46	49.8	145.06	583	7.7
S6 BAZ 210	240	2012	8	27	43719.43	12.14	-88.59	28	7.3
S7 BAZ 337	227	2012	8	14	25938.46	49.8	145.06	583	7.7
S7 BAZ 210	240	2012	8	27	43719.43	12.14	-88.59	28	7.3
S8 BAZ 337	227	2012	8	14	25938.46	49.8	145.06	583	7.7
S8 BAZ 204	249	2012	9	5	144207.88	10.1	-85.31	35	7.6
S9 BAZ 337	227	2012	8	14	25938.46	49.8	145.06	583	7.7
S9 BAZ 204	249	2012	9	5	144207.88	10.1	-85.31	35	7.6
S10 BAZ 261	103	2012	4	12	71548.62	28.624	-113.116	13	7
S10 BAZ 230	80	2012	3	20	180247.45	16.499	-98.224	20	7.4
S11 BAZ 261	103	2012	4	12	71548.62	28.624	-113.116	13	7
S11 BAZ 230	80	2012	3	20	180247.45	16.499	-98.224	20	7.4

Table 3 Cont'd

Receiver Function	Event Description								
	YearDay	YEAR	MONTH	DAY	ORIG TIME	LAT	LONG	DEPTH	MAG
S12 BAZ 261	103	2012	4	12	71548.62	28.624	-113.116	13	7
S12 BAZ 230	80	2012	3	20	180247.45	16.499	-98.224	20	7.4
HRV BAZ 261	103	2012	4	12	71548.62	28.624	-113.116	13	7
HRV BAZ 180	58	2010	2	27	80123.01	-37.77	-75.05	35	7.4
	70	2010	3	11	145527.51	-34.33	-71.8	18	7
	2	2011	1	2	202017.78	-38.3	-73.33	24	7.2
	85	2012	3	25	223706	-35.2	-72.22	40	7.1
S13 BAZ 261	103	2012	4	12	71548.62	28.624	-113.116	13	7
S13 BAZ 230	80	2012	3	20	180247.45	16.499	-98.224	20	7.4
S13 BAZ 180	85	2012	3	25	223706	-35.2	-72.22	40	7.1
	108	2012	4	17	35015.61	-32.62	-71.36	29	6.7
WES BAZ 316	199	2010	7	18	55644.93	52.88	-169.85	14	6.7
	175	2011	6	24	30939.47	52.05	-171.84	52	7.3
	245	2011	9	2	105553.59	52.17	-171.71	32	6.9
WES BAZ 172	247	2008	9	3	112514.45	-26.74	-63.22	569	6.3
	1	2011	1	1	95658.12	-26.8	-63.14	576	7
	245	2011	9	2	134709.62	-28.4	-63.03	578	6.7
	149	2012	5	28	50723.45	-28.04	-63.09	586	6.7

Appendix 4: Seismic Resolution

Sheriff and Geldart (1995) define resolution as the minimum separation between two features such that one can tell from the seismic data that that there are two features rather than one. In seismology, resolution is divided into vertical resolution and horizontal resolution.

Vertical resolution

Vertical resolution is determined using the Rayleigh Criterion, which defines the minimum vertical separation between two horizontal beds such that the wave arrivals from each bed do not interfere constructively (Figure A5). The minimum vertical separation required is one quarter the wavelength (λ/4).

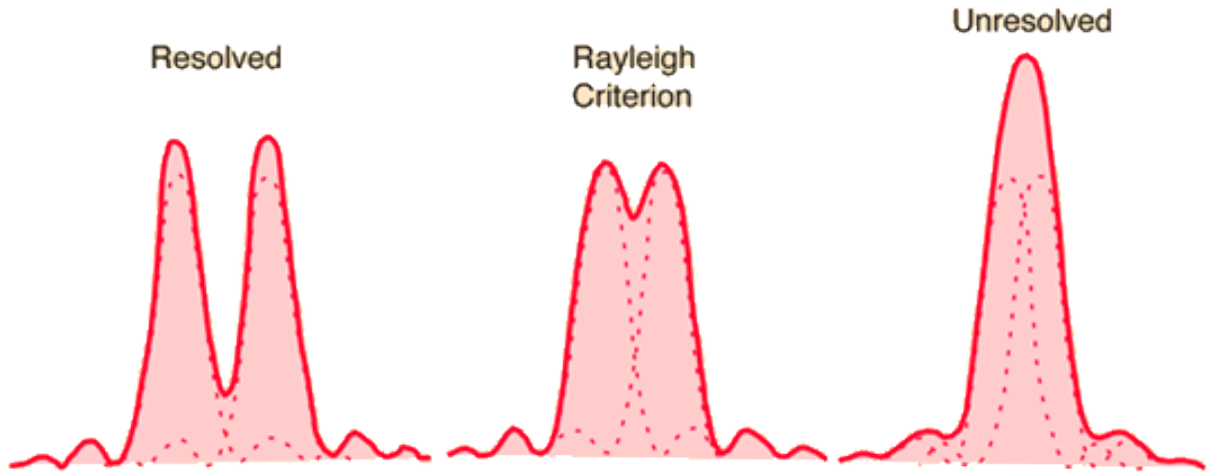

Figure A6. Illustration of the Rayleigh criterion. On the far left, the arrivals shown are from two horizontal layers that are more than 1-quarter wavelength apart. In the center, the arrivals are exactly one-quarter wavelength apart. On the far right, the arrivals are less than one-quarter wavelength apart and interfere constructively. Figure from Hyperphysics educational website, © C.N. Nave, 2012. (http://hyperphysics.phyastr.gsu.edu/hbase/phyopt/raylei.html)

The Gaussian width parameter used to create receiver functions determines the pulse width of the wave arrivals that are analyzed. A Gaussian width parameter of 2.5 was used, which

translates to a pulse width of ≈1 second in the receiver functions. Using the Rayleigh Criterion as an estimate of error, the vertical resolution of these 0.5 Hz receiver functions is ±0.9km.

Horizontal Resolution

Traveling wave reflections and transitions are generally modeled as rays in seismology. However, the reflections or conversions are made up of energy arriving from a fairly large area (Sheriff and Geldart, 1995). The Fresnel zone defines the horizontal area from which the energy arriving at a station has phases differing by no more than a half-cycle, which should interfere constructively. The radius of the Fresnel zone (Fr) is given as

$$Fr = (v/2)(t/f)$$

where v is the seismic velocity, t is the travel time from the source to the receiver, and f is the dominant wave frequency. The outer portion of the Fresnel zone makes little contribution to the result (Sheriff and Geldart, 1995), so the effective Fresnel radius (Fe) is often used:

$$Fe \approx Fr/\sqrt{2}$$

The dominant frequency of teleseismic body waves is expected to be ≈1Hz (Foley, 1990; Levander, 2003). Using expected ak135 travel time and velocity of Ps waves in the crust, the horizontal resolution in this study is ≈3.9 km for the Moho and ≈2.7 km for the mid-crust.